Atmos. Meas. Tech., 8, 4429–4451, 2015
www.atmos-meas-tech.net/8/4429/2015/
doi:10.5194/amt-8-4429-2015

Atmospheric Measurement Techniques
Open Access
EGU

The direct fitting approach for total ozone column retrievals: a sensitivity study on GOME-2/MetOp-A measurements

A. Wassmann, T. Borsdorff, J. M. J. aan de Brugh, O. P. Hasekamp, I. Aben, and J. Landgraf

Netherlands Institute for Space Research SRON, Sorbonnelaan 2, 3584 CA Utrecht, the Netherlands

Correspondence to: A. Wassmann (a.wassmann@sron.nl)

Received: 23 March 2015 – Published in Atmos. Meas. Tech. Discuss.: 13 May 2015
Revised: 28 September 2015 – Accepted: 12 October 2015 – Published: 21 October 2015

Abstract. We present a sensitivity study of the direct fitting approach to retrieve total ozone columns from the clear sky Global Ozone Monitoring Experiment 2/MetOp-A (GOME-2/MetOp-A) measurements between 325 and 335 nm in the period 2007–2010. The direct fitting of the measurement is based on adjusting the scaling of a reference ozone profile and requires accurate simulation of GOME-2 radiances. In this context, we study the effect of three aspects that introduce forward model errors if not addressed appropriately: (1) the use of a clear sky model atmosphere in the radiative transfer demanding cloud filtering, (2) different approximations of Earth's sphericity to address the influence of the solar zenith angle, and (3) the need of polarization in radiative transfer modeling. We conclude that cloud filtering using the operational GOME-2 FRESCO (Fast Retrieval Scheme for Clouds from the Oxygen A band) cloud product, which is part of level 1B data, and the use of pseudo-spherical scalar radiative transfer is fully sufficient for the purpose of this retrieval. A validation with ground-based measurements at 36 stations confirms this showing a global mean bias of -0.1 % with a standard deviation (SD) of 2.7 %. The regularization effect inherent to the profile scaling approach is thoroughly characterized by the total column averaging kernel for each individual retrieval. It characterizes the effect of the particular choice of the ozone profile to be scaled by the inversion and is part of the retrieval product. Two different interpretations of the data product are possible: first, regarding the retrieval product as an estimate of the true column, a direct comparison of the retrieved column with total ozone columns from ground-based measurements can be done. This requires accurate a priori knowledge of the reference ozone profile and the column averaging kernel is not needed. Alternatively, the retrieval product can be interpreted as an effective column defined by the total column averaging kernel. This interpretation relies much less on the a priori knowledge of the reference ozone profile; however, for its validation, measurements of the vertical ozone distribution are needed. The different manners of data interpretation are demonstrated for simulated and real measurements using on-ground ozone column and ozonesonde measurements for validation.

1 Introduction

Ozone is an important constituent of Earth's atmosphere, and monitoring its atmospheric abundance is essential to improve our understanding on tropospheric chemistry, air quality and climate change (e.g., Guicherit and Roemer, 2000; WHO, 2003; WMO, 2014; Fuhrer, 2009; Fleming et al., 2011). For this purpose, satellite measurements in the ultraviolet (UV) part of the solar spectrum between 310 and 340 nm form a valuable tool in measuring the vertically integrated amount of ozone with global coverage. The Global Ozone Monitoring Experiment 2 (GOME-2) (Munro et al., 2015) aboard the three European sun-synchronous, polar-orbiting MetOp satellites, with two currently in operation and the third one due for launch in 2017, measures earth radiance and solar irradiance spectra in the UV, visible, and near-infrared spectral range from 240 to 790 nm with a spectral resolution of 0.24–0.53 nm and a spectral sampling of 0.11–0.22 nm. It continues a long history starting with the Solar Backscatter Ultraviolet instruments (SBUV and SBUV/2) (Bhartia et al., 1996) and the Total Ozone Mapping Spectrometer (TOMS) (Bhartia and Wellemeyer, 2004) on Nim-

bus 7 launched in 1978, followed in Europe by GOME (Burrows et al., 1999) on ERS-2 in 1995, the Scanning Imaging Absorption Spectrometer for Atmospheric CHartographY (SCIAMACHY) (Bovensman et al., 1999) on Envisat in 2002, and the Ozone Monitoring Instrument (OMI) (Levelt, 2006) on Aura in 2004.

To retrieve total ozone columns from these instruments, different algorithms have been developed. Most of the algorithms employ the Differential Optical Absorption Spectroscopy (DOAS) technique (e.g., Coldewey-Egbers et al., 2005; Weber et al., 2005; Eskes et al., 2005; Van Roozendael et al., 2006; Veefkind et al., 2006; Loyola et al., 2011), which is beneficial with respect to its computational cost. For GOME-2, the operational O3MSAF/EUMETSAT (European Organisation for the Exploitation of Meteorological Satellites) ozone column product is based on the DOAS method implemented in the GOME Data Processor version GDP v4.7 (Hao et al., 2014) and is extensively validated with ground-based measurements. Antón et al. (2009) performed a validation for total ozone columns retrieved with GDP v4.2 over the Iberian Peninsula using Brewer spectrometer measurements and found a bias of $-3.05\,\%$, while Loyola et al. (2011) report a global mean bias and standard deviation (SD) of $-0.28 \pm 0.7\,\%$ with respect to Dobson spectrometer measurements and $-1.22 \pm 0.67\,\%$ with respect to Brewer spectrometer measurements for total ozone columns retrieved with GDP v4.4. A comparison with the total ozone columns from GOME (processor version GDP v4.1), SCIAMACHY (processor version SGP v5.0), and OMI (processor versions TOMSv8.5 and DOAO3v1.0.1 and level 1b data version collection 3) showed biases of -0.8, -0.37, $-1.28\,\%$, respectively, when compared with GOME-2 (processor version GDP v4.4 and level 1b data version 4), ensuring a consistent data set (Koukouli et al., 2012). Furthermore, degradation of satellite instruments in the UV is often observed (e.g., GOME, Snel , 2000; Tanzi et al., 2000; van der A et al., 2002, and SCIAMACHY, Noël et al., 2007; Bramstedt et al., 2009). Several methods have been published to correct measured reflectances with modeled reflectances (e.g., van der A et al., 2002; Krijger et al., 2005; van Soest et al., 2005) or by comparing measured reflectances to those at the beginning of the mission after removing both solar zenith angle and seasonal dependencies (Liu et al., 2007; Tilstra et al., 2012a). Cai et al. (2012) provide an extensive analysis of both the spectral and the cross-track degradation of GOME-2 measurements with time compared with model simulations and derived an empirical radiometric correction.

As an alternative to the DOAS retrieval approach, Lerot et al. (2010) and Van Roozendael et al. (2012) proposed the direct fitting approach for the retrieval of total ozone columns. In this approach GOME UV radiance measurements are fitted using a non-linear least squares fitting algorithm to adjust a scaling of a reference ozone profile. During the iteration the vertical profile is adjusted on the basis of the total-ozone-column-classified TOMS climatology (e.g., Bhartia and Wellemeyer, 2002; McPeters et al., 2007). An important aspect of the direct fitting approach is the simulation of the GOME measurement during the iteration using a physical model based on atmospheric radiative transport. Lerot et al. (2014) adapted the tropospheric part of the climatology from the climatology of Ziemke et al. (2011) and implemented the calculation of total column averaging kernels. The direct fitting of satellite radiance measurements to determine atmospheric trace gas columns is also successfully applied in the retrieval CO columns from SCIAMACHY measurements (e.g., Gloudemans et al., 2008), CH_4 and CO_2 columns from the Greenhouse Gases Observing Satellite (GOSAT) (e.g., Butz et al., 2011) or in CO column retrievals from simulated Sentinel-5 and Sentinel-5P measurements (Vidot et al., 2012).

In this study, we investigate aspects of the direct fitting approach by using an implementation similar to the algorithm of Lerot et al. (2014). In particular we focus on two aspects: first, the relevance of forward model errors of the measurement simulations and, second, the role of the regularization due to the scaling of the reference profile. For this purpose, we present an algorithm which adapts the total column amount of the reference ozone profile, whose relative shape is kept fixed during the iteration. This modification of the approach of Lerot et al. (2014) is chosen to better analyze the effect of the regularization. As part of a least squares profile scaling approach, we simulate clear sky earth radiances using solar spectra, which are retrieved beforehand from GOME-2 solar irradiance measurements. The algorithm performance is evaluated by means of a validation with ground-based Brewer, Dobson and Système d'Analyse par Observation Zénithale (SAOZ) spectrometer data and collocated ozonesonde measurements considering a correction for the altitude of the validation site and the degradation of the satellite instrument. The effects of satellite instrument degradation on the earth radiance measurements are partly mitigated by a radiometric correction that we derived for the first 4 years of the mission from global cloud-free measurements referenced to 2007, which is the first year of the mission. Moreover, we address forward model errors such as an error introduced by residual cloud contamination in a clear sky retrieval due to poor cloud filtering, the representation of Earth's sphericity and the appropriate choice of the radiative transfer solver, considering vector and scalar radiative transfer solvers. Finally, we highlight the aspect of regularization using the total column averaging kernel to interpret the error introduced by the choice of the reference ozone profile.

The paper is structured as follows: in Sect. 2 we briefly describe the forward model and the inversion scheme. Section 3 describes the radiometric correction of the GOME-2 measurements to mitigate the instrument degradation. In Sect. 4 we present the performance analysis followed by a forward model error study. Finally, we address the aspect of regularization in Sect. 5 and conclude the paper in Sect. 6.

2 Algorithm description and retrieval setup

2.1 Forward model

To retrieve total ozone columns from GOME-2 measurements, a forward model $\mathbf{F}_{\text{earth}}$ is needed in order to simulate GOME-2 earth radiance measurements $\boldsymbol{y}_{\text{earth}}$ as

$$\boldsymbol{y}_{\text{earth}} = \mathbf{F}_{\text{earth}}(\boldsymbol{x}, \boldsymbol{b}) + e_{\text{earth}}. \quad (1)$$

$\mathbf{F}_{\text{earth}}$ is a function of the state vector $\boldsymbol{x}$ to be retrieved and the model parameter vector $\boldsymbol{b}$, which contains additional parameters that influence the spectrum but are not altered by the inversion. The error vector e_{earth} combines both errors in the measurement and forward model errors.

The forward model $\mathbf{F}_{\text{earth}}$ requires a solar spectrum $\boldsymbol{S}_0$ sampled on an internal, fine spectral grid. To infer $\boldsymbol{S}_0$ from the daily GOME-2 solar irradiance measurements $\boldsymbol{y}_{\text{sun}}$, we set up a forward model equation analogous to Eq. (1) but for the solar measurement, where we assume that the solar measurement $\boldsymbol{y}_{\text{sun}}$ can be simulated by spectral convolution of the solar spectrum $\boldsymbol{S}_0$ with the instrument spectral response function. This yields the forward model equation for the solar spectrum

$$\boldsymbol{y}_{\text{sun}} = \mathbf{K}_{\text{ISRF}}\boldsymbol{S}_0 + e_{\text{sun}}. \quad (2)$$

The matrix $\mathbf{K}_{\text{ISRF}}$ represents the convolution of the solar spectrum with the instrument spectral response function and e_{sun} is the corresponding error vector. In Eq. (2), the length of the observation vector $\boldsymbol{y}_{\text{sun}}$ is smaller than the length of $\boldsymbol{S}_0$, so its inversion has no unique solution. Van Deelen et al. (2007) showed that the least squares minimum length solution $\hat{\boldsymbol{S}}_0$, which minimizes the length of the solution vector $\hat{\boldsymbol{S}}_0$ as a side constraint, is of sufficient accuracy to simulate earth radiance measurements of the GOME mission. Following this approach using GOME-2 solar measurements as disseminated by EUMETSAT, we calculate the earth radiance measurements by

$$\mathbf{F}_{\text{earth}}(\hat{\boldsymbol{S}}_0) = \mathbf{K}_{\text{ISRF}}(\boldsymbol{r} \cdot \hat{\boldsymbol{S}}_0), \quad (3)$$

where we explicitly show the dependence of $\mathbf{F}_{\text{earth}}$ on the solar spectrum and omit any other dependence. Furthermore, $\boldsymbol{r}$ is the spectral reflectance of Earth's atmosphere. Equation (3) assumes the same instrument spectral response function for solar irradiance and earth radiance measurements, so the noise contribution on the inferred solar spectrum $\hat{\boldsymbol{S}}_0$ is attenuated by the convolution in Eq. (3). In the present study we use a Gaussian instrument spectral response function with a full width at half maximum of 0.3 nm.

The transfer of light through Earth's atmosphere is described by the reflectance $\boldsymbol{r}$ as part of the convolution

$$(\boldsymbol{r} \cdot \hat{\boldsymbol{S}}_0)(\lambda) = \int \mathrm{d}\widetilde{\lambda}\, r(\lambda, \widetilde{\lambda})\hat{\boldsymbol{S}}_0(\widetilde{\lambda}). \quad (4)$$

It includes the description of inelastic Raman scattering and elastic Rayleigh scattering of solar light, where the integral kernel $r(\lambda, \widetilde{\lambda})$ represents the reflection of sunlight at the incoming wavelength $\widetilde{\lambda}$ to the outgoing wavelength λ. Numerical calculations of $\boldsymbol{r}$ are very time-consuming (e.g., Landgraf et al., 2004; van Deelen et al., 2005) and thus require an approximation to keep the numerical effort of the algorithm reasonable. Based on the concept of pre-calculated ring spectra (e.g., Hoogen et al., 1999; Hasekamp and Landgraf, 2001; Lerot et al., 2014), we approximate Eq. (4) by

$$(\boldsymbol{r} \cdot \hat{\boldsymbol{S}}_0) \approx \boldsymbol{r}_{\text{Ray}} \cdot \hat{\boldsymbol{S}}_0 \left(1 + a \frac{\boldsymbol{r}^{\text{LUT}}_{\text{Ram}} \cdot \hat{\boldsymbol{S}}_0}{\boldsymbol{r}^{\text{LUT}}_{\text{Ray}} \cdot \hat{\boldsymbol{S}}_0}\right), \quad (5)$$

where $\boldsymbol{r}_{\text{Ray}}$ is the monochromatic earth reflectance due to atmospheric Rayleigh scattering. It is calculated online employing the LINTRAN radiative transfer model (Landgraf et al., 2001; Walter et al., 2004; Hasekamp et al., 2005; Schepers et al., 2014). For all simulations, we use ozone cross sections by Brion et al. (1993), which are calculated for the given temperature profile, as well as scattering cross sections and phase matrices for Rayleigh scattering described by Bucholtz (1995). LINTRAN comprises a scalar and vector radiative transfer solver in plane parallel geometry and its pseudo-spherical extension. In this study, we employ the scalar solver with the pseudo-spherical approximation if not mentioned differently. Additionally, $\boldsymbol{r}^{\text{LUT}}_{\text{Ray}}$ and $\boldsymbol{r}^{\text{LUT}}_{\text{Ram}}$ are pre-calculated reflectances stored in a lookup table, which includes Rayleigh scattering and inelastic Raman scattering, respectively. The lookup table is calculated with the model by Landgraf et al. (2004) for the US standard atmosphere (NOAA, 1976) assuming a nadir viewing geometry, solar zenith angles between 10 and 80° in 10° steps, a Lambertian surface albedo $A_{\text{s}} = 0.1$, and total ozone columns between 280 and 400 DU in steps of 20 DU. Here, the solar zenith angle dependence of the lookup table is chosen because atmospheric Ring spectra depend significantly on this parameter (see e.g., Joiner et al., 1995). The lookup table also includes the dependence on the total amount of ozone to avoid interference of the filling-in of ozone absorption features in the Huggins band due to atmospheric Raman scattering with the retrieved total column of ozone. Factor a in Eq. (5) is a free model parameter to adjust the effect of Raman scattering in the retrieval.

The use of the reflectance lookup tables $\boldsymbol{r}^{\text{LUT}}_{\text{Ram}}$ and $\boldsymbol{r}^{\text{LUT}}_{\text{Ray}}$ in Eq. (5) instead of pre-calculated Ring spectra bears the advantage that the simulation is based on one solar spectrum, which eases the spectral calibration of the forward model. Assuming the molecular spectroscopy of ozone as spectral reference, the forward model can be spectrally adjusted by shifting the solar spectrum in Eq. (5), $\hat{\boldsymbol{S}}_0(\lambda) \rightarrow \hat{\boldsymbol{S}}_0(\lambda + \Delta\lambda_{\text{S}})$, to account for the Doppler shift and furthermore to serve as a means of spectral calibration of the solar spectrum. A corresponding spectral adjustment of the instrument spectral response function $s(\lambda, \widetilde{\lambda}) \rightarrow s(\lambda + \Delta\lambda_{\text{ISRF}}, \widetilde{\lambda})$ accounts for a

spectral shift between absorption features of the earth radiance simulation and the GOME-2 measurement. Both spectral shift parameters $\Delta\lambda_S$ and $\Delta\lambda_{ISRF}$ are independent elements of the state vector and are determined by the inversion module, which is discussed in the next section.

To simulate the sensitivity of the modeled spectrum to the parameters of the state vector, we use the linearization capability of LINTRAN, which provides the derivatives of $\boldsymbol{r}_{Ray}$ with respect to absorption and scattering parameters of the model atmosphere. We approximate the derivatives $\partial\mathbf{F}_{earth}/\partial\tau_j$ with respect to the absorption optical thickness τ_j in model layer j by

$$\frac{\partial\mathbf{F}_{earth}}{\partial\tau_j} \approx \mathbf{K}_{ISRF}\left(\frac{\partial\boldsymbol{r}_{Ray}}{\partial\tau_j}\cdot\hat{\boldsymbol{S}}_0\left(1+a\,\frac{\boldsymbol{r}^{LUT}_{Ram}\cdot\hat{\boldsymbol{S}}_0}{\boldsymbol{r}^{LUT}_{Ray}\cdot\hat{\boldsymbol{S}}_0}\right)\right), \tag{6}$$

and a corresponding expression $\partial\mathbf{F}_{earth}/\partial A_s$ holds for the derivative with respect to the spectral Lambertian surface albedo A_s. The derivatives with respect to the amplitude a in Eq. (5) can be calculated analytically in a straightforward manner. Moreover, for the Gaussian instrument spectral response function, the derivative $\partial\mathbf{F}_{earth}/\partial\Delta\lambda_{ISRF}$ can be derived analytically, whereas the derivatives $\partial\mathbf{F}_{earth}/\partial\Delta\lambda_S$ are determined numerically using finite differences.

2.2 Inversion module

For the inversion, we need to linearize the forward model around an initial guess of the state vector $\boldsymbol{x}_0$,

$$\boldsymbol{y} = \mathbf{K}\boldsymbol{x} + e_{earth}, \tag{7}$$

where $\mathbf{K} = \partial\mathbf{F}_{earth}/\partial\boldsymbol{x}$ is the Jacobian matrix and $\boldsymbol{y} = \boldsymbol{y}_{earth} - \mathbf{F}_{earth}(\boldsymbol{x}_0, \boldsymbol{b}) + \mathbf{K}\boldsymbol{x}_0$. To retrieve the total ozone column, we follow the profile scaling approach used by Lerot et al. (2010). The state vector consists of the total ozone column c, the surface albedo A_0 at a reference wavelength λ_0 and its spectrally linear dependence δA, with $A_s(\lambda) = A_0 + \delta A(\lambda - \lambda_0)$, the amplitude a in Eq. (5), a spectral shift of the solar spectrum $\Delta\lambda_S$, and a spectral shift of the instrument spectral response function $\Delta\lambda_{ISRF}$ in Eq. (3). Here, the column density c is defined by vertical profile integration,

$$c = \mathbf{C}^T\boldsymbol{\rho}, \tag{8}$$

where $\mathbf{C} = (1, \ldots, 1)$ represents the corresponding geometric integration assuming an ozone profile $\boldsymbol{\rho}$ given in partial column densities per model layer.

We apply Eq. (7) to invert Eq. (1) in an iterative way with respect to the state vector $\boldsymbol{x}$ using Gauss–Newton iteration, for which the minimization problem

$$\hat{\boldsymbol{x}} = \min_x\left\{\left\|\mathbf{S}_e^{-1/2}(\mathbf{K}\boldsymbol{x} - \boldsymbol{y})\right\|_2^2\right\} \tag{9}$$

is solved in each iteration step. Here $\|\cdot\|_2$ represents the L_2 norm and $\mathbf{S}_e$ is the measurement error covariance. For this purpose, the Jacobian with respect to a scaling of a reference profile is calculated from corresponding derivatives with respect to an altitude-resolved ozone profile $\boldsymbol{\rho}$,

$$\boldsymbol{K}^{col}_i = \frac{\partial\mathbf{F}_{earth,i}}{\partial c} = \sum_j \mathbf{K}^{prof}_{ij}\frac{\boldsymbol{\rho}^{ref}_j}{c^{ref}}. \tag{10}$$

Here, $\mathbf{K}^{prof}_{ij} = \partial\mathbf{F}_{earth,i}/\partial\rho_j = \sigma_i\partial\mathbf{F}_{earth,i}/\partial\tau_j$ describes the profile Jacobian at a wavelength i, where ρ_j is the ozone subcolumn in model layer j and σ_i the corresponding ozone absorption cross section. Furthermore, $\boldsymbol{\rho}^{ref}$ is the reference profile used for the scaling approach. From Eq. (10) it is clear that the profile scaling approach relies on an altitude-resolved profile Jacobian. A direct analytical calculation of the derivative $\partial\mathbf{F}_j/\partial c$ is not possible due to scattering and the temperature dependence of the ozone absorption. $\mathbf{K}^{col}$ together with the derivatives of the measurement with respect to the other elements of the state vector defines the column of the least squares Jacobian $\mathbf{K}_{lsq}$ and the solution of Eq. (9) is given by

$$\hat{\boldsymbol{x}} = \mathbf{G}_{lsq}\boldsymbol{y} \tag{11}$$

with the gain matrix

$$\mathbf{G}_{lsq} = \left(\mathbf{K}^T_{lsq}\mathbf{S}_e^{-1}\mathbf{K}_{lsq}\right)^{-1}\mathbf{K}^T_{lsq}\mathbf{S}_e^{-1}. \tag{12}$$

The least squares scaling approach can be interpreted as a regularized retrieval of the vertical ozone distribution (Borsdorff et al., 2014). Hence, the retrieved column $\hat{c}$ represents an estimate of an altitude-weighted integration of the true ozone profile, namely

$$\hat{c} = \mathbf{A}^{col}\boldsymbol{\rho}_{true} + e_{col}, \tag{13}$$

where $\mathbf{A}^{col}$ is the total column averaging kernel, $\boldsymbol{\rho}_{true}$ is the true ozone profile and e_{col} is the error on the retrieved column due to the measurement error e_y. This means that generally the retrieved column $\hat{c}$ should be interpreted as an estimate of the effective column

$$c_{eff} = \mathbf{A}^{col}\boldsymbol{\rho}_{true}. \tag{14}$$

The part of the true column that cannot be inferred from the measurement, namely

$$e_n = (\mathbf{C} - \mathbf{A}^{col})\boldsymbol{\rho}_{true}, \tag{15}$$

belongs to the effective null space of the inversion and is also known as smoothing error of the retrieval (Rodgers, 2000). Borsdorff et al. (2014) discussed the meaning of e_n in terms of the profile scaling approach. Interpreting the effective column c_{eff} as an estimate of the true column, e_n represents the error made by the choice of the reference profile $\boldsymbol{\rho}_{ref}$ to be scaled in the inversion. Obviously, when the reference profile represents the correct relative vertical trace gas distribution,

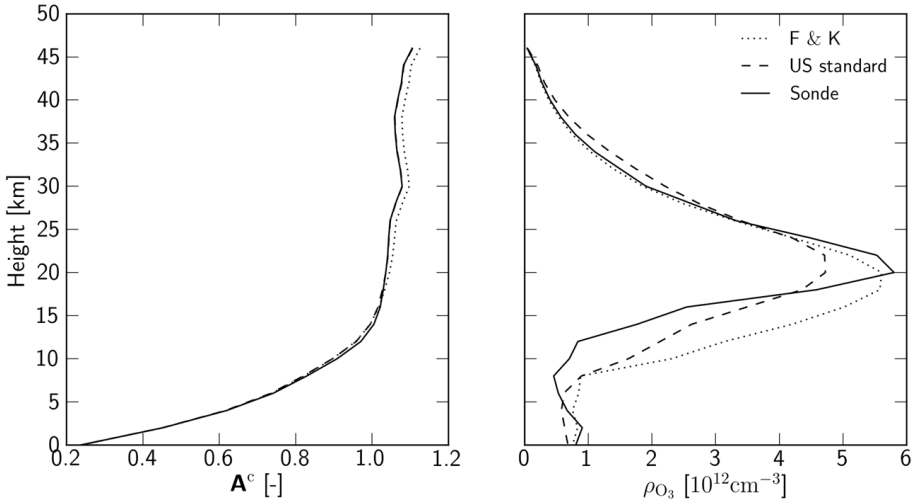

Figure 1. Left panel: total column averaging kernel using the ozone profile of the US standard atmosphere (dashed), from the climatology by Fortuin and Kelder (1998) (dotted), and the ozonesonde profile from 15 January 2009 over De Bilt, the Netherlands (solid). The right panel shows the corresponding ozone profiles. The measurements are simulated for a cloud-free scene, the ozonesonde profile and a solar zenith angle of 70°, a viewing zenith angle of 30°, and a surface albedo of 0.1.

e_n vanishes. Therefore, e_n does not reflect an erroneous interpretation of the measurement but originates from a wrong a priori knowledge of the vertical ozone profile. For data interpretation and validation it is desirable to disentangle both error sources.

Consequently, two different conclusions with respect to the interpretation of the profile scaling approach can be drawn: (1) aiming for an estimate of the true column, it has to be stressed that accurate a priori knowledge on the relative vertical distribution of $\boldsymbol{\rho}_{\mathrm{ref}}$ has to be provided. In that case, the column averaging kernel is not needed for a proper data interpretation. This interpretation is adapted by Lerot et al. (2010) and further elaborated by Lerot et al. (2014), where the reference profile is updated during the iteration using the empirical correlation between the total amount of ozone and its vertical distribution (Ziemke et al., 2011). (2) Alternatively, one can focus on the information provided by the measurement and consider Eq. (14) as the definition of the retrieval product, where the total column averaging kernel describes a weighted altitude integration of the vertical ozone profile. Here, the effective null space error is not part of the error budget of the product and the retrieval depends much less on a priori profile information. However, the proper data use requires detailed knowledge and application of the column averaging kernel.

The comparison of both views on the data product in the context of the product validation is one aspect of this study. For validation purposes, following the first interpretation the retrieved column can be directly compared to total ozone columns inferred from ground-based spectrometer measurements, which are recorded routinely as part of a global measurement network, while for the second interpretation the vertical distribution of ozone needs to be known. For the latter, ozonesonde measurements can be used. However, due to fewer observation sites and less frequent measurements, a corresponding validation is limited in its spatiotemporal coverage. On the other hand, the advantage of this approach is the minor dependence of the data product on the a priori knowledge of the vertical ozone distribution. Important applications, like the assimilation of the total ozone column in global and regional models, preferably deal with information purely coming from the measurements and thus try to minimize the effect of ozone knowledge originating from a priori data. For such applications, the effective column together with its total column averaging kernel forms a well-suited data product.

To infer the total column averaging kernel in our algorithm, we follow the approach by Borsdorff et al. (2014). Interpreting the profile scaling approach as a particular case of a regularized profile retrieval using Tikhonov regularization of the first order (i.e., using the first derivative of the vertical profile with respect to altitude in the regularization matrix) with an "infinitely strong" regularization, Borsdorff et al. (2014) showed that the gain matrix reduces to a gain vector $\boldsymbol{g}^{\mathrm{col}}$ representing the fitted ozone column. Moreover, we can extract $\boldsymbol{g}^{\mathrm{col}}$ from the gain matrix of the least-squares fit $\mathbf{G}_{\mathrm{lsq}}$ and calculate the total column averaging kernel

$$\mathbf{A}^{\mathrm{col}} = \left(\frac{\mathrm{d}c}{\mathrm{d}\boldsymbol{\rho}_i}\right) = \boldsymbol{g}^{\mathrm{col}}\mathbf{K}^{\mathrm{prof}}. \tag{16}$$

For the proof of Eq. (16), the reader is referred to Borsdorff et al. (2014).

Figure 1 shows the total column averaging kernels for retrievals from simulated measurements. Here, the mea-

surements are simulated for a cloud-free scene and an ozonesonde profile on 15 January 2009 over De Bilt, the Netherlands, representing the true ozone profile. Retrievals are performed for three different reference ozone profiles: the US standard ozone profile (NOAA, 1976); the corresponding profile extracted from the climatology by Fortuin and Kelder (1998), which provides monthly averaged climatological ozone profiles in 10° latitude bands; and the true ozone profile itself. All are depicted in the right panel of Fig. 1 as a dashed line, dotted line, and solid line, respectively. Although the US standard and the climatological reference profile of Fortuin and Kelder (1998) peak at different altitudes with different magnitudes, one can see in the left panel that the general shape of the total column averaging kernel is largely similar. The null space contribution of the sonde profile clearly differs for the given model atmosphere and is $e_n = 0.12\,\%$ for the US standard ozone profile and $e_n = -0.95\,\%$ for the climatological profile, respectively. It vanishes when the ozonesonde profile itself is used as reference profile as expected. Depending on the reference profiles, we thus can expect errors on the order of 1 % for moderate solar zenith angles when we interpret the retrieved column as an estimate of the true column. For low solar elevation at high latitude stations in winter the error can even amount to 5 %. This error source can be avoided when we interpret the retrieved column as an effective column and subsequently apply the total column averaging kernel concept for validation. In Sect. 5 we demonstrate this aspect by applying both concepts to GOME-2 measurements.

3 Instrument degradation

To validate the presented algorithm, we apply it to spectra recorded by GOME-2/MetOp-A between January 2007 and July 2011, disseminated by EUMETSAT. Due to the choice of the retrieval window between 325 and 335 nm, we only use data from channel 2B with the advantage of the small 80×40 km ground pixels. Because of the optical degradation of the GOME-2 scan mirror, the reflectance measurements are subject to a spectral radiometric error. To mitigate this error, two major approaches are reported in the literature, one based on the predictability of the measurement using radiative transfer simulations and a priori knowledge about the atmospheric state and the other based on actual measurements, assuming that the averaged radiometric signal over certain regions is constant for the same period of the year, i.e., surface albedo and observation geometry. For example, Cai et al. (2012) calculate the degradation as the relative difference between measured data and modeled data in the wavelength region between 270 and 350 nm for the tropical belt (25° S–5° N), where ozone varies only little, for the period between February 2007 and December 2009 in 15-day intervals. For GOME, Liu et al. (2007) presented a different approach comparing measured reflectances with respect to those of a reference date. Assuming a constant mean reflectance value, they considered the mean reflectance measured between 60° N and 60° S as a function of time for the first and 15th day of each month. Subsequently, the mean reflectance is referenced to the value determined for 1 July 1995. To remove solar zenith angle dependency and other seasonality, two third-order polynomials in time are fitted to the data. The approach assumes a constant state of the atmosphere and does not account for long-term trends in the total amount of ozone. Pawson et al. (2014) determined an average trend of $0.08 \pm 0.13\,\%$ per year for the period 2000–2013. This introduces a small uncertainty in the derived radiometric degradation. There are also several advantages of using observations only over a comparison with simulated measurements. First, no collocations of the radiative transfer input parameters with the measurements are needed and, second, more importantly, uncertainties in ozone profiles, temperature profiles, and cloud data which lead to forward model errors are avoided. In that way only the effect of the instrument degradation and of atmospheric variations remain. However, averaging daily data over a large enough region reduces the impact of the latter.

In this paper, we follow a similar approach to Liu et al. (2007), monitoring degradation at three wavelengths in our total ozone fitting window, namely 325, 330, and 335 nm. For each of the wavelengths, we consider GOME-2 reflectances for the forward viewing geometry of the descending node between 60° N and 60° S with minor cloud contamination of cloud fraction $f_{\mathrm{cld}} \leq 10\,\%$, which is calculated by the FRESCO cloud algorithm (Wang et al., 2008) and disseminated as part of the GOME-2 level 1B product. We arrange the data in 5° latitude bins, 2° solar zenith angle bins, and 24 ground pixel bins representing the cross-track scan. To define the degradation δI_{deg} for the period 2008–2011, the reflectance is referenced to the corresponding reflectance of the year 2007, which is also the first year of the mission, on the same day of the year for the same solar zenith angle bin, latitude bin and ground pixel bin. We observe a clear scan angle dependence, shown for 330 nm in Fig. 2. Here, ground pixel 1 represents the easternmost pixel and ground pixel 24 represents the westernmost pixel. One can clearly identify different rates at which the across-track degradation takes place as indicated by the color gradients. The westward pixels are subject to the most severe degradation with about 9.5 % at the end of the period under investigation, while the eastward pixels are least affected (3–4 %), which is comparable to the findings of Tilstra et al. (2012b). Cai et al. (2012) report a cross-track-dependent degradation ranging from 0.6 % to less than 2.2 % from east to west pixels at 325 nm after 3 years. Based on these findings, we correct the relative radiometric degradation of GOME-2 radiances with respect to solar measurements assuming a multiplicative error contribution (R. Snel, personal communication, 2014, SRON, the Netherlands). Since the degradation showed only little spectral dependency across our fitting window, we consider it

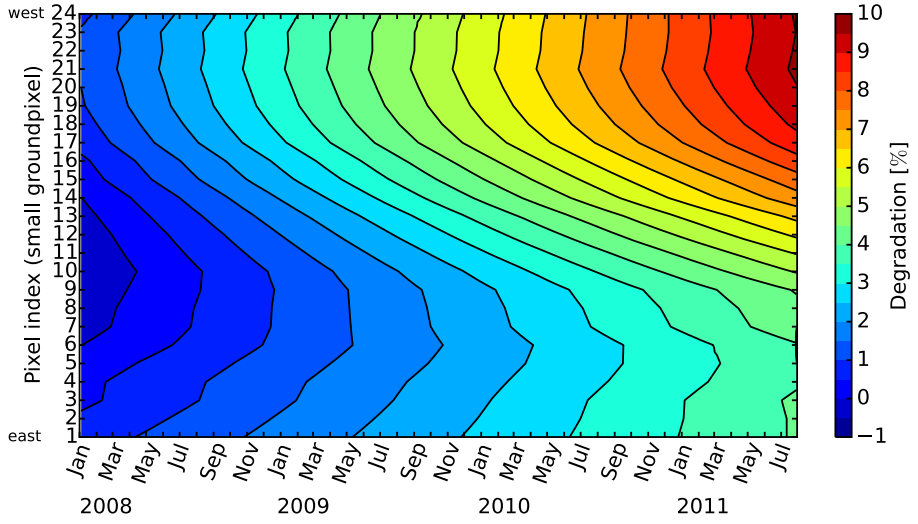

Figure 2. Degradation of globally averaged reflectances with respect to reference year 2007 per small ground pixel at 330 nm in the ozone fitting window (325–335 nm). Ground pixel 1 is the easternmost pixel of a scan and pixel 24 is the westernmost pixel.

spectrally constant. From the data of Fig. 2, we derived a corresponding degradation correction for the period 2008–2011 per scan mirror position by linear regression. It is assumed that the GOME-2 data are not affected by the degradation in 2007 and hence are not corrected.

4 Performance analysis

In this section, we carry out a performance analysis of our direct fitting approach. Different aspects of the forward model that impact the quality of the retrieval product such as residual cloud contamination in clear sky radiative transfer modeling, the representation of Earth's sphericity and thus the dependency on solar zenith angles, and the need of polarization in radiative transfer modeling are discussed. For this evaluation, we directly compare the retrieved column with ground-based measurements using reference ozone profiles extracted from the climatology by Fortuin and Kelder (1998). Furthermore, we use temperature and pressure profiles from the European Centre for Medium-Range Weather Forecasts (ECMWF) ERA-Interim data (Berrisford et al., 2009) as auxiliary input and define a filter to reject retrievals in cloudy atmospheres. This cloud filter is based on FRESCO cloud parameters (Wang et al., 2008), which are part of the disseminated GOME-2 level 1B product, and is discussed in detail in Sect. 4.1. For a proper comparison, ground-based data have to be recorded on the same day and be spatially co-aligned. Additionally, we corrected the total column from ground-based measurements for the difference in surface elevation between the measurement site and the mean GOME-2 pixel elevation, which is derived from Shuttle Radar Topography Mission (SRTM) high-resolution digital topographic database (Farr et al., 2007) and the near-surface ozone mixing ratio approximated by the ozone reference profile.

In total, we consider ozone measurements at 36 stations and extracted the corresponding data from the World Ozone and Ultraviolet Radiation Data Centre (WOUDC; see www.woudc.org) and the Southern Hemisphere ADditional OZonesondes (SHADOZ; Thompson et al., 2007) networks. The stations are listed in Table 1 together with their location and the type of the ground-based instrumentation. For some stations, more than one ground-based instrument was operational for the examined period, which allows us to intercompare different instrumentations. Furthermore, Table 1 indicates a good coverage of validation sites in the Northern Hemisphere with an even higher density of stations in Europe.

In this section, we compare ground-based ozone column measurements with collocated GOME-2 ozone columns directly. To reduce the effect of regularization in this comparison, we use the ozone climatology by Fortuin and Kelder (1998) to extract appropriate reference profiles. The algorithm validation depends also on the accuracy of the ground-based total column measurements of ozone. Fioletov et al. (2008) indicated less accuracy of zenith sky measurements and so we exclude these measurements in our study. Moreover, Basher (1982), Komhyr et al. (1989), Basher (1994), Kerr et al. (1997), and Fioletov et al. (2005) reported that a precision of 1 % for well-calibrated Brewer and Dobson instruments can be reached. However, systematic differences of about ± 0.6 % between both are introduced through different temperature dependencies of the absorption cross sections at the different wavelengths used by the instruments (Staehelin et al., 2003). Furthermore, Bernhard et al. (2005) stated that a fixed stratospheric temperature and the parameterization of the ozone layer in total ozone retrievals from

Table 1. Number of measurements N, biases b and error SD (σ) of the validation for each station. Data set 1 comprises the results of the direct column comparison described in Sect. 4 using profiles from the climatology by Fortuin and Kelder (1998) as reference profiles and the filter criteria $\delta t < 30$ DU, $\delta r < 300$ km, $\chi^2 \leq 2$, and $\eta_{\mathrm{cld}} < 0.1$ are applied. Data set 2 comprises the results of the effective column comparison using ozonesonde profiles as reference and the more stringent filter criterion $\delta t < 15$ DU, while the other remain as for data set 1.

Station name	Lat.	Long.	Instrument	Data set 1			Data set 2		
				N	b [%]	σ [%]	N	b [%]	σ [%]
Alert	82.5° N	62.3° W	B-MKII.019	121	0.9	3.0	7	0.2	3.0
Eureka	80.1° N	86.2° W	B-MKV.069	130	−0.7	2.4	13	−1.1	1.1
Resolute	74.7° N	95.0° W	B-MKII.031	166	−0.4	3.3	7	0.4	1.4
Scoresbysund	70.5° N	22.0° W	SAOZ[a]	164	3.2	3.5	13	4.2	2.8
Lerwick	60.1° N	1.2° W	D-Beck.032	85	0.1	2.6	8	−0.3	2.2
Churchill	58.8° N	94.0° W	B-MKII.026	155	0.5	3.5	18	0.6	4.8
			B-MKIV.032	17	2.2	4.8	137	1.3	3.7
Edmonton	53.6° N	114.1° W	B-MKII.055	290	−0.1	2.5	24	−0.9	2.0
			B-MKIV.022	236	−0.1	2.9	25	−0.5	3.0
Goose Bay	53.3° N	60.4° W	B-MKII.018	209	0.7	2.5	15	0.7	2.7
Lindenberg	52.2° N	14.1° E	B-MKII.030	96	−0.9	2.3	10	−0.1	2.7
De Bilt	52.1° N	5.2° E	B-MKIII.189	202	−1.3	1.8	17	−1.0	1.8
Valentia Obs.	51.9° N	10.3° W	B-MKIV.088	150	−0.5	2.2	10	−0.6	2.9
Uccle	50.8° N	4.4° E	B-MKII.016	172	0.3	2.1	33	0.5	2.5
			B-MKIII.178	177	0.2	2.0	40	0.5	1.8
Praha	50.0° N	14.5° E	D-Beck.070	79	−0.7	2.3	5	1.4	2.7
			B-MKIII.184	207	−1.0	2.2	6	0.0	2.0
			B-MKIV.098	222	−0.9	2.4	7	0.4	2.1
Hohenpeißenberg	47.8° N	11.0° E	B-MKII.010	215	−0.3	1.8	49	−0.6	1.9
Egbert	44.2° N	79.8° W	B-MKII.015	274	0.2	3.5	26	0.2	2.8
OHP	43.9° N	5.7° E	D-Beck.085	38	0.5	2.3	9	−0.1	2.2
			SAOZ[a]	327	−0.0	2.5	29	0.1	2.5
Sapporo	43.1° N	141.3° E	D-Beck.126	177	0.6	3.0	15	−1.0	1.9
Madrid	40.5° N	3.6° W	B-MKIV.070	184	−1.1	2.2	16	−0.8	2.9
Boulder	40.1° N	105.3° W	D-Beck.082	161	0.8	2.9	22	1.1	2.5
Ankara	40.0° N	32.9° E	B-MKIII.188	280	0.2	2.3	11	−0.2	1.6
Tateno	36.1° N	140.1° E	D-Beck.125	145	1.0	3.1	14	1.9	2.7
Izaña	28.3° N	16.5° W	B-MKIII.157[a]	342	0.2	1.7	36	−0.6	1.4
Naha	26.2° N	127.7° E	D-Beck.127	409	−0.6	2.1	47	0.1	1.7
Hong Kong Obs.	22.3° N	114.2° E	B-MKIV.115	376	−1.2	1.8	36	1.0	2.0
Mauna Loa[b]	19.6° N	155.1° W	D-Beck.076	205	1.1	1.6	28	1.2	1.7
Paramaribo	5.8° N	55.2° W	B-MKIII.159	482	−0.3	1.2	48	−0.3	1.1
Sepang Airport	2.7° N	101.7° E	B-MKII.090	338	0.0	2.2	22	0.5	2.5
Samoa	14.3° S	170.6° W	D-Beck.042	33	0.9	1.7	–	–	–
Reunion Island	21.0° S	55.5° E	SAOZ[a]	620	0.0	1.5	58	0.4	1.7
Broadmeadows	37.7° S	145.0° E	D-Beck.115	305	−1.1	4.0	26	−0.1	2.5
Lauder	45.0° S	169.7° E	D-Beck.072	108	−1.1	4.2	–	–	–
Macquarie Island	54.5° S	159.0° E	D-Beck.006	71	−2.3	4.2	5	0.5	2.8
Ushuaia	54.9° S	68.3° W	D-Beck.131	71	1.2	3.4	–	–	–
Marambio	64.2° S	56.7° W	D-Beck.099	99	3.3	2.9	6	0.7	1.7
Dumont d'Urville	66.7° S	140.0° E	SAOZ[a]	216	1.6	4.2	9	0.3	3.8
Syowa	69.0° S	39.6° E	D-Beck.119	56	−0.6	2.7	5	−1.0	2.8
Global				6861	−0.1	2.7	647	0.1	2.5

[a] No observation mode was given, so all available data that meet the collocation criteria were used. [b] In data set 2, collocated ozonesondes from the station Hilo are used.

Dobson spectrometers cause both seasonal and solar zenith angle dependencies of the ground-based measurements of up to 4 %. For SAOZ instruments, Van Roozendael et al. (1998) carried out a validation with Dobson and Brewer instruments and found a bias of about 2 % between the two types of measurements. Thus, differences between GOME-2 retrieval and

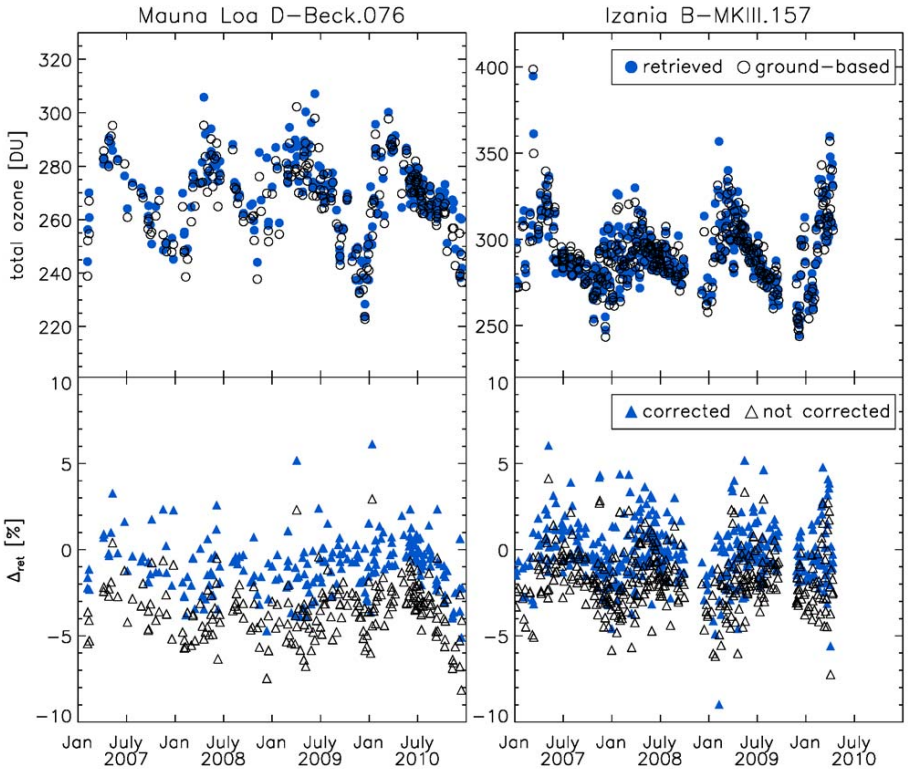

Figure 3. Time series of total ozone columns and the retrieval error. Upper panels: the retrieved ozone column (filled blue circles) and the ground-based measurements using the elevation correction (open circles) for the sites Izaña and Mauna Loa. Lower panels: retrieval error of the time series corrected and not corrected for elevation differences between satellite ground pixel and measurement site (filled blue and open triangles, respectively).

ground-based measurements have to be considered in the view of this overall uncertainty of our validation measurements.

4.1 Data filtering

For the performance analysis and the subsequent validation we define and apply four quality criteria for data selection. First, we define a cloud filter to select GOME-2 measurements with minor cloud contamination based on an effective cloudiness parameter:

$$\eta_{\mathrm{cld}} = f_{\mathrm{cld}} \frac{z_{\mathrm{cld}}}{z_{\mathrm{ref}}}, \tag{17}$$

where f_{cld} is the factional cloud coverage of the observed scene, z_{cld} the cloud top height and z_{ref} a reference height. The effective cloudiness parameter yields largest values for high clouds and large cloud fraction and thus describes a shielding of the subjacent atmosphere. For the numerical implementation of the cloud screening, we employ the GOME-2 FRESCO cloud product (Wang et al., 2008), which is part of the level 1B product, and assume a reference height $z_{\mathrm{ref}} = 10\,\mathrm{km}$. Second, assuming the spatiotemporal variation of ozone to be ergodic, we use its temporal variation to filter spatial heterogeneity around the validation sites. Therefore, we consider 3 days of consecutive ground-based measurements, with the second day being spatiotemporally coregistered with a GOME-2 measurement. The difference of that collocated ground-based measurement with the ground-based measurements of the preceding day and succeeding day (δt) has to be less than a threshold value. Although the ergodic assumption on the ozone variation may not hold in general and thus may lead to too strict data filtering, it is used to identify spatial heterogeneity in ozone, which is laterally transported over the observed scene. Third, measurements are assumed to be spatially co-aligned when the distance between the site of the ground-based measurements and the center of the GOME-2 pixel δr does not exceed a threshold. Finally, only GOME-2 products with $\chi^2 \leq \chi^2_{\mathrm{max}}$ of the spectral fitting are considered, where

$$\chi^2 = \frac{1}{N-1} \sum_{i=1}^{N} [(\boldsymbol{r}_{\mathrm{meas}}(i) - \boldsymbol{r}_{\mathrm{mod}}(i))/\sqrt{\mathbf{S}_{\mathrm{e}}(i,i)}]^2 . \tag{18}$$

Here, $\boldsymbol{r}_{\mathrm{meas}}$ and $\boldsymbol{r}_{\mathrm{mod}}$ are the measured and simulated reflectance, respectively, and N is the number of spectral measurements. For the evaluation of our data product, we choose

the following quality filtering:

$$\delta t < 30 \text{ DU}, \quad (19)$$

$$\delta r < 300 \text{ km}, \quad (20)$$

$$\chi^2_{\text{max}} = 2, \quad (21)$$

$$\eta_{\text{cld}} < 0.1\,. \quad (22)$$

For this data filtering, we find 6861 collocations between all ground-based measurements and GOME-2 observations.

4.2 Topography correction and instrument degradation correction

Before validating our data product with ground-based measurements, we introduce two important corrections. First, we correct the ground-based measurements of the total ozone column for topographic differences between the validation site and the satellite ground pixel, despite then excluding those stations, which is commonly done (e.g., Fioletov et al., 2008). Figure 3 demonstrates the relevance of this correction for the elevated sites Izaña (∼ 2300 m a.s.l.) and Mauna Loa (∼ 3400 m a.s.l.). Here, we obtain mean biases of 0.2 and 1.1 % after correction, compared to −1.8 and −3.5 %, respectively, without elevation correction. For other stations, the elevation correction is of minor importance due to smaller differences in elevation.

Second, we consider a radiometric correction for the GOME-2 instrument degradation of the UV radiance measurements, which is known to be an important issue for data interpretation (e.g., Snel , 2000; Tanzi et al., 2000; van der A et al., 2002 and SCIAMACHY Noël et al., 2007; Bramstedt et al., 2009). We investigate the influence of the scan-angle-dependent degradation with time on the retrieved total ozone columns and omit the wavelength-dependent degradation since it is small across the 325–335 nm fitting window. For that purpose, we perform a validation of retrieved total ozone columns calculated from GOME-2 measurements with and without the degradation correction, which is described in Sect. 3 for a subset of collocated ground stations. The subset comprises the stations Ankara, Churchill (Brewer MKII.026), De Bilt, Edmonton (Brewer MKII.055), Hohenpeißenberg, Hong Kong Observatory, Izaña, Naha, and Paramaribo, and is chosen such that it includes measurements at different latitudes and provides good data coverage for every single station in the investigated period.

Figure 4 (top panel) shows an improvement in the validation in the last third of the time series, covering the period from September 2009 to December 2010, of ∼ 0.5 % when the degradation correction is applied (red bars). Attributed to our approach of determining the degradation, no difference between retrievals with and without degradation correction is seen in 2007, since this year serves as reference as discussed earlier. Therefore, the relative degradation of the GOME-2 reflectance measurements δI_{deg} is zero in 2007, seen in the middle panel which shows the mean radiometric

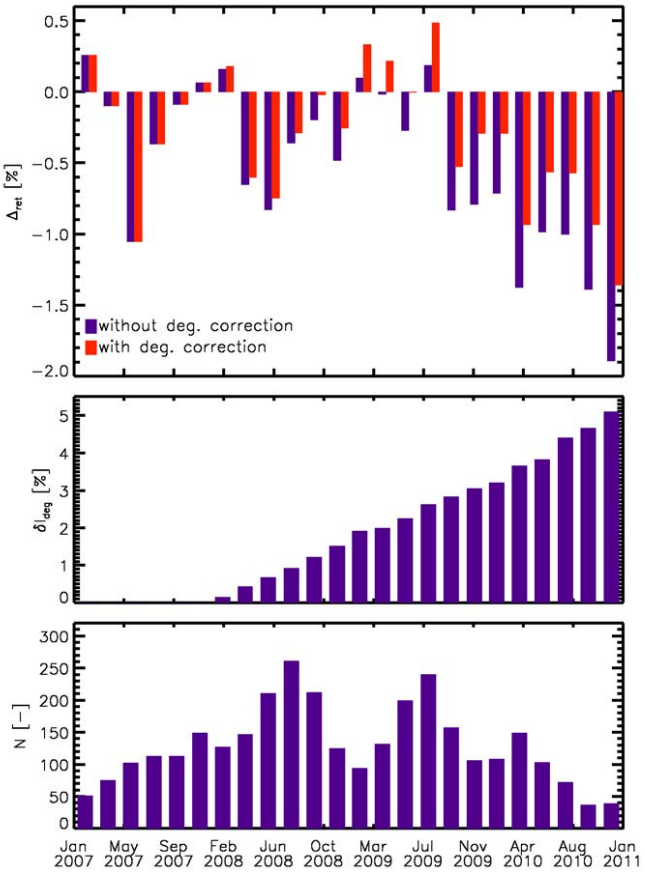

Figure 4. Top panel: time series of the total ozone column retrieval error (Δ_{ret}) with (red) and without (blue) degradation correction. Middle panel: degradation for the corresponding bin referenced to 2007. Bottom panel: data abundance for each bin. The data are acquired from collocations with Ankara, Churchill (Brewer MKII.026), De Bilt, Edmonton (Brewer MKII.055), Hohenpeißenberg, Hong Kong Observatory, Izaña, Naha, and Paramaribo.

degradation averaged over the corresponding 2-month bin in the time series. The biases seen in the top panel show more variation which might be related to the choice of the validation sites, their instrumentation and the data coverage over the period under investigation, which is shown in the lower panel of the figure. However, in the context of biases of 0.6 % between Brewer and Dobson instruments (Staehelin et al., 2003) and 2 % between SAOZ and both Brewer and Dobson instruments (Van Roozendael et al., 1998), the biases that we report are close to or within the limits of the validation.

Next, we investigate the scan angle dependency of the degradation and its influence on the retrieved product. We aggregate the data set into 6-month bins of east and west pixels by dividing between eastwards (pixel index 1–12) and westwards (pixel index 13–24) scans in order to obtain meaningful statistics. Figure 5 shows that the retrieval error increases faster for the uncorrected western pixels (light blue) than for the eastern pixels (dark blue). Comparing the uncorrected re-

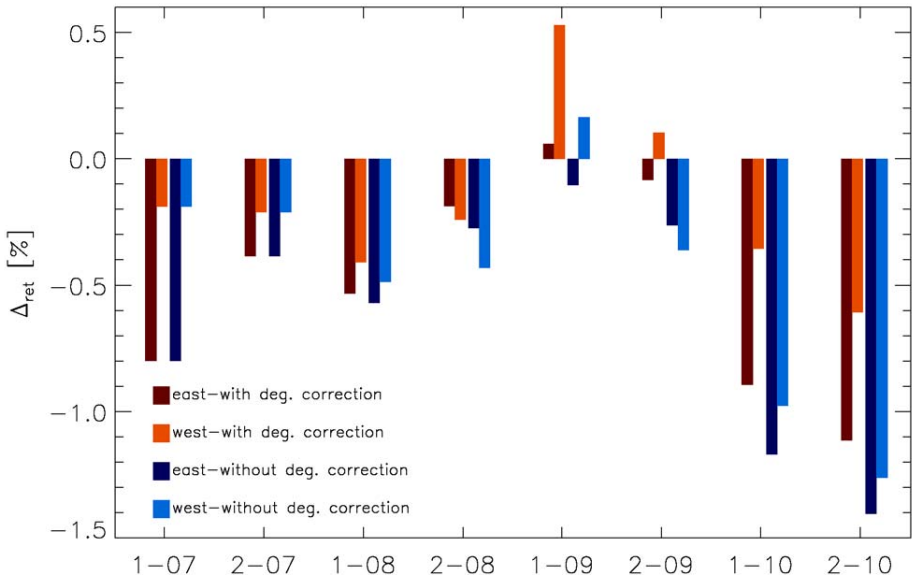

Figure 5. Influence of the scan-angle-dependent degradation on the total ozone column retrieval error (Δ_{ret}). Data are binned into 6-month intervals as well as east and west pixel bins, which include pixel numbers 1–12 and 13–24 (Fig. 2). The lighter colors indicate the western pixels and the darker colors the eastern pixels. Furthermore, blue colors represent the data not corrected for degradation and the orange and brown colors the degradation-corrected data. The underlying data set is the same as in Fig. 4.

trievals with their corrected counterpart, western pixels in orange and eastern pixels in brown, this becomes even more obvious. The spurious features seen here in the beginning of the time series are of the same origin as in Fig. 4. Because these errors already occur in the beginning of the time series, especially the difference between west and east pixels may hint at a radiometric calibration bias of the eastward pixels. From Fig. 5 we conclude that applying the degradation correction to the west pixels improves the retrieval error in the validation with ground-based instruments from $\Delta_{ret} = -1.3\,\%$ to $\Delta_{ret} = -0.6\,\%$ at the end of the investigated 4-year period, while the correction of the east pixels has a smaller effect. A difference in total ozone columns of about 1.5–2 % between the west and east pixels is also reported by (e.g., Antón et al., 2009; Loyola et al., 2011; Koukouli et al., 2012; Hao et al., 2014). Hence, the application of the degradation correction improves the validation in that interval and is expected to become even more important for the ongoing mission beyond the period that we investigated.

4.3 Forward model errors

This section focuses on the relevance of forward model errors for our retrieval product. First, we consider the effect of the remaining cloud contamination after data filtering assuming a clear sky atmosphere in the forward simulation. Subsequently, we study the effect of Earth's sphericity and its approximation in the radiative transfer model and, finally, we evaluate the effect of scalar radiative transfer approximation for the retrieval of the total ozone column.

4.3.1 Cloudiness

Clouds significantly affect the light path through the atmosphere. Depending on the cloud optical properties, cloud morphology and surface properties, the light path can be shortened or enhanced compared to the clear sky situation (e.g., Pfeilsticker et al., 1998). Using satellite measurements, clouds are typically characterized by effective cloud parameters, which describe the light path for the considered spectral range. For GOME-2, cloud parameters are commonly retrieved from the O_2 A band at around 760 nm (e.g., FRESCO cloud parameters; Wang et al., 2008). The adaptation of these cloud parameters for a correct light path simulation in the UV is not obvious (van Diedenhoven et al., 2007). Because of this, we decided to rely on clear sky observations requiring a cloud filtering of the GOME-2 observations in the current version of our algorithm and proposed the cloud filtering of GOME-2 observations based on the cloudiness parameter η_{cld}, defined in Eq. (17). To demonstrate the validity of this filtering, we consider the ozone column retrieval error as a function of the cloudiness parameter η_{cld} and discard the cloudiness threshold set in Eq. (22). In this way we obtain 9600 valid data points. Next, we determine a bias from nearly cloud-free scenes ($\eta_{cld} < 0.1$) for each station and correct the corresponding data set for it. The determined bias reflects other error sources which may depend on the particular site and are in this way disentangled from the error due to cloudiness. This correction varies between ±2 % depending on the validation site, which is also reflected in the station-to-station bias variation in the left column of Table 1. Apply-

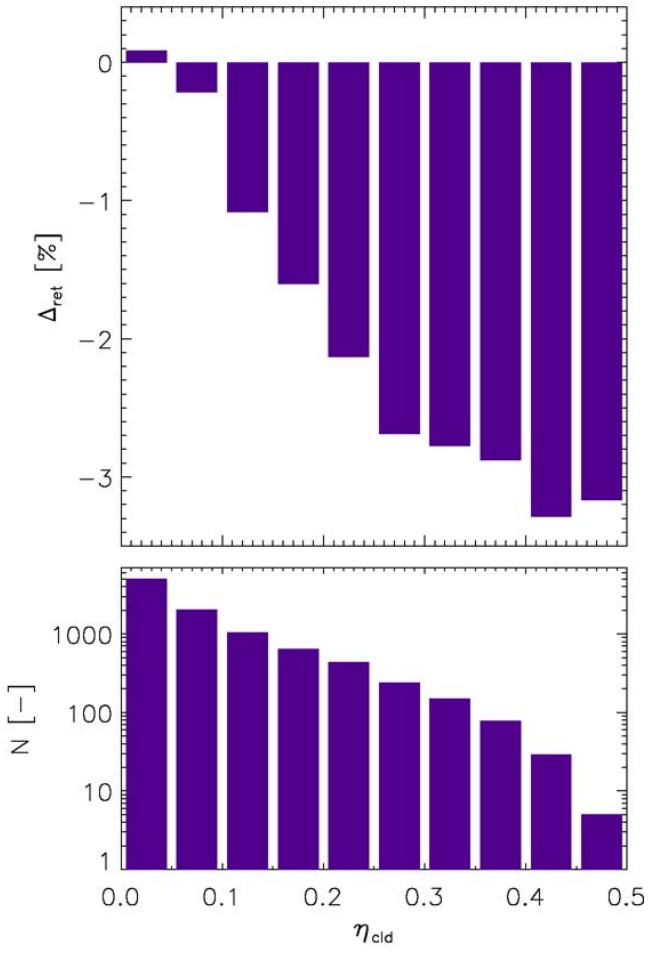

Figure 6. Mean retrieval error as function of the cloudiness parameter η_{cld} (Eq. 17) aggregated into bins of $\eta_{cld} = 0.05$. Upper panel: the mean retrieval error in percent. Lower panel: number of data points per bin of cloudiness. In total, the data set comprises 9600 data points.

ing this correction highlights the dependence of the retrieval bias on cloudiness η_{cld} as shown in Fig. 6. For $\eta_{cld} \leq 0.1$ the relative dependence on cloudiness is weak but increases significantly for $\eta_{cld} > 0.1$, showing already a retrieval error of about $-1\,\%$ for $\eta_{cld} = 0.15$ and further increases to $\Delta_{ret} = -3.2\,\%$ for $\eta_{cld} = 0.5$. This justifies the use of the clear sky radiative transfer simulation in conjunction with cloud filtering as proposed in Eq. (22) in Sect. 4.1.

4.3.2 Earth's sphericity

For satellite observations at large solar zenith angles, the treatment of Earth's sphericity as part of the radiative transfer simulation becomes an important aspect. To select a proper approach for our retrieval problem, we investigated the retrieval performance as a function of solar zenith angle for three different approximations: plane-parallel approximation, the air mass correction of Kasten and Young (1989) and the pseudo-spherical approximation (Walter et al., 2004). Here, we selected validation sites for which the GOME-2 measurements cover at least the range of 50–80° solar zenith angles. Similarly to the disentanglement of the cloudiness error in Sect. 4.3.1, we separate the error due to the influence of the solar zenith angle from other error sources. To do so, each station of the data set is corrected for its mean bias determined from solar zenith angles $\theta < 55°$, which varies between -2 and $3\,\%$. In this way, we consider the relative error at larger solar zenith angles. Figure 7 shows a clear improvement when using the pseudo-spherical approximation instead of the plane-parallel approximation with and without air mass correction. For $\theta > 70°$, using the plane-parallel approximation underestimates the ozone column up to a mean error of $7.5\,\%$ at $\theta = 85°$. Errors are reduced by more than a factor 2 using the air mass correction and reduce to about $-0.5\,\%$ for pseudo-spherical approximation. This is in agreement with the sphericity effect studied for simulated measurements and suggests using the pseudo-spherical approximation for our retrieval.

Nevertheless, the relative error shows some suspicious features, e.g., the positive error of $2\,\%$ for the pseudo-spherical simulations at $\theta = 77°$. This may be caused by the fact that the underlying data set of this study consists of Brewer, Dobson, and SAOZ measurements with different solar zenith angle dependencies. Due to the sampling of different solar zenith angle ranges of the measurements at different stations, features can be introduced. For a better comprehension of the satellite solar zenith angle dependence of the retrieval, Fig. 8 shows the retrieval error as function of the solar zenith angle for the Praha Dobson spectrometer (left) and the Praha Brewer MKIV.098 spectrometer (right). For both data sets, we identify a potential trend by linear regression. The SD of the data points with respect to the regression is used to characterize the overall quality of the regression. Although being situated at the same validation site and hence GOME-2 covers the same range of solar zenith angles, the data sets show different dependences. The Dobson instrument shows a clear positive trend with increasing solar zenith angle of $1\,\%$ per 10° solar zenith angle, whereas for the Brewer instrument such a trend is not present in the data ($0.1\,\%$). Thus for Praha, we conclude that the error trend is probably inflicted by the ground measurements and not by the GOME-2 data, so one may suggest that the Praha Dobson spectrometer is more susceptible to solar zenith angle dependencies than Brewer instruments, which is also shown by Bernhard et al. (2005). Table 2 summarizes the slope of the regression and the SD for all stations of Table 1 with sufficient data coverage. Significant slopes are observed for the stations Churchill (B-MKIV.032), Goose Bay, Praha (Dobson), Boulder, Tateno, and Ushuaia, which is confirmed by the small variation of the SD of the data points around the linear regression within the data set. The trends in Table 2 indicate a significant error dependence on solar zenith angle for Dob-

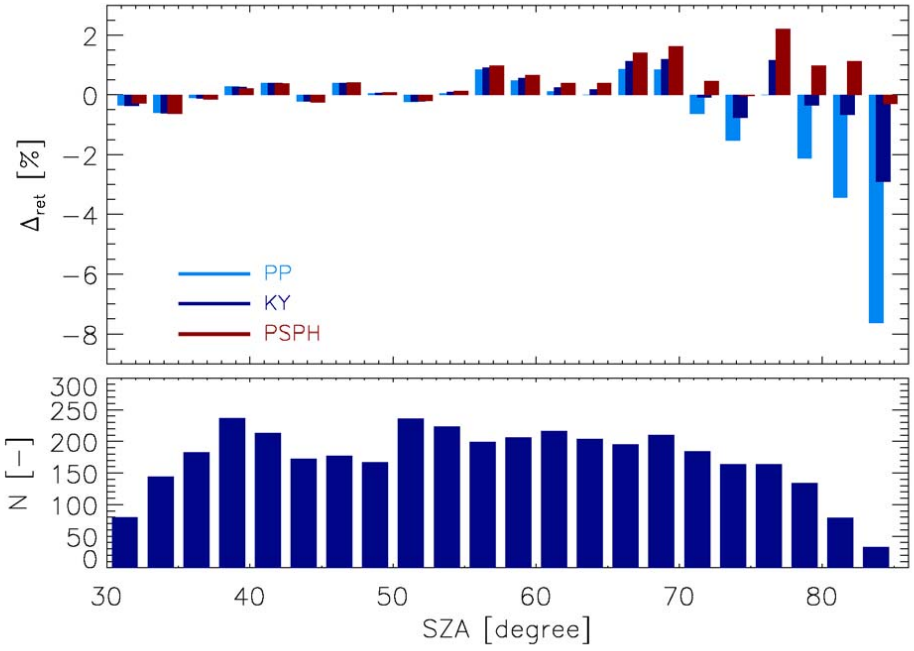

Figure 7. Mean ozone retrieval error as a function of solar zenith angle θ for different approximations of Earth's sphericity in the radiative transfer calculation. Upper panel: the mean ozone retrieval error in percent for the plane parallel approximation (PP, light blue), air mass correction of Kasten and Young (1989) (KY, dark blue), and pseudo-spherical approximation (Walter et al., 2004) (PSPH, red). Lower panel: number of data points per 2.5° bin of θ. The validation set comprises cloud-free measurements at Resolute, Churchill B-MKII.026, Edmonton B-MKII.055, Lindenberg, Macquarie Island, Dumont d'Urville, and Goose Bay (see Table 1 for more details about the different sites). For each measurement site, the data are corrected for an overall bias for solar zenith angles $\theta < 55$.

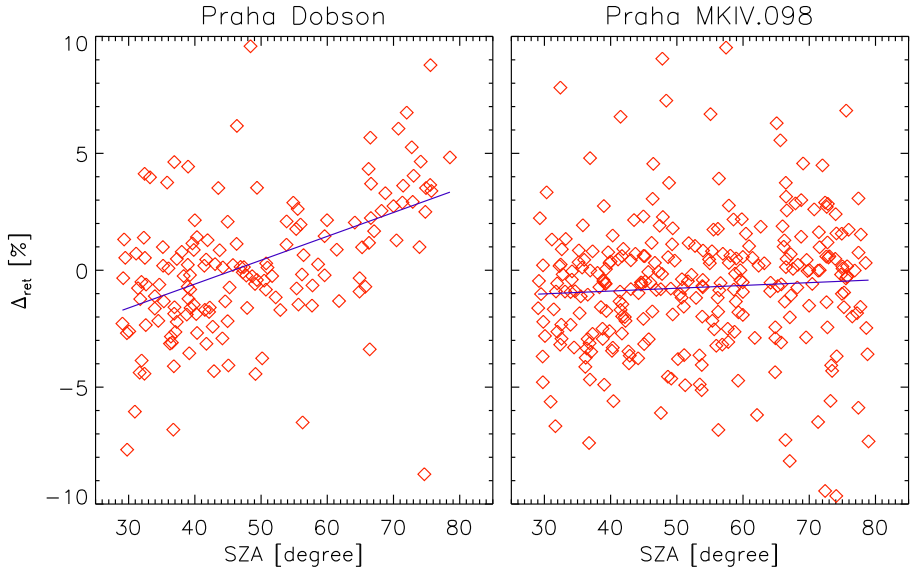

Figure 8. Retrieval error Δ_{ret} as function of solar zenith angle θ for the Praha Dobson (D-Beck.070) (left) and the Praha Brewer spectrometers (B-MKIV.098) (right). The blue lines are trends determined by linear regression.

Table 2. Linear dependence of the retrieval error Δ_{ret} on solar zenith angle θ, characterized by the slope m of a linear regression through the data point per 10° of solar zenith angle (see also Fig. 8) and the SD (σ) around the linear regression.

Station name	Lat.	Long.	Instrument	m [% (10°)$^{-1}$]	σ [%]
Lerwick	60.1° N	1.2° W	D-Beck.032	1.2	3.3
Churchill	58.8° N	94.0° W	B-MKIV.032	0.98	4.3
Edmonton	53.6° N	114.1° W	B-MKII.055	0.36	2.85
Goose Bay	53.3° N	60.4° W	B-MKII.018	0.74	3.18
De Bilt	52.1° N	5.2° E	B-MKIII.189	0.16	1.89
Uccle	50.8° N	4.4° E	B-MKII.016	0.2	2.67
Uccle	50.8° N	4.4° E	B-MKIII.178	0.19	2.44
Praha	50.0° N	14.5° E	D-Beck.070	0.97	2.96
Praha	50.0° N	14.5° E	B-MKIV.098	0.11	3.13
OHP	43.9° N	5.7° E	D-Beck.085	−0.38	2.11
OHP	43.9° N	5.7° E	SAOZ	−0.19	2.73
Sapporo	43.1° N	141.3° E	D-Beck.126	0.17	4.24
Boulder	40.1° N	105.3° W	D-Beck.082	0.8	4.22
Tateno	36.1° N	140.1° E	D-Beck.125	0.83	3.93
Izaña	28.3° N	16.5° W	B-MKIII.157	0.5	1.72
Hong Kong Obs.	22.3° N	114.2° E	B-MKIV.115	−0.18	3.06
Mauna Loa	19.6° N	155.1° W	D-Beck.076	0.66	1.83
Sepang Airport	2.7° N	101.7° E	B-MKII.090	−0.18	7.11
Reunion Island	21.0° S	55.5° E	SAOZ	0.29	1.5
Ushuaia	54.9° S	68.3° W	D-Beck.131	1.07	4.81

son spectrometers, confirming the findings of Bernhard et al. (2005).

4.3.3 The scalar radiative transfer approximation

Due to multiple scattering of solar light in the ultraviolet spectral range, correct radiance simulations have to take the polarization of scattered light into account at the cost of numerically expensive simulations. Neglecting polarization by scalar radiative transfer introduces errors in the modeled radiances, which can be as large as 10 % depending on the scattering geometry of the singly scattered light (Mishchenko et al., 1994; Stammes , 1994; Lacis et al., 1998). Consequently, one may argue that the use of the scalar radiative transfer solver in our LINTRAN forward model potentially causes retrieval biases depending on scattering geometry and subsequently on the solar zenith angles. In the left panel of Fig. 9, the spectral error in the wavelength ranges between 303 and 336 nm and is shown for different solar geometries and comprises a strong wavelength dependence for wavelengths smaller than 320 nm for almost all investigated scattering geometries. Here, the polarization of light is governed by singly scattered light, which for Rayleigh scattering has its highest degree of linear polarization for a scattering angle of $\Theta_{scat} = 90°$. Thus, polarization affects the intensity at higher scattering orders and consequently causes an error on the simulated intensity if not accounted for. For the spectral window used in this study (325–335 nm), this error comprises mainly a radiometric offset but it also includes spectral features interfering with spectral absorption features of ozone, which is shown in the right panel for the same scattering geometry. To estimate the effect of the used scalar forward model on our retrieved ozone column product, we have generated synthetic measurements for the whole range of satellite solar and viewing geometries of the validation data set for Lerwick using the LINTRAN vector radiative transfer model. The retrieval errors in the total ozone columns caused by the scalar radiative transfer approximation are shown in Fig. 10 as function of the scattering angle in single scattering geometry. In case we fit a spectrally constant effective albedo, as shown in the left panel, the error on the total ozone column is substantial with a maximum of 4 % at a scattering angle $\Theta_{scat} = 90°$, where the maximum error is expected to be. Here, the error pattern clearly follows the radiometric offset in Fig. 9. The retrieval error induced by using the scalar version of the forward model can be further reduced by fitting a linear spectrally dependent surface albedo, which is depicted in the right panel of Fig. 10. For almost all scattering angles the error diminishes and is below 0.7 % in all cases.

Although the effect of these forward model errors is small, it is interesting to see if the use of vector radiative transfer in the retrieval of total ozone columns improves the validation with ground measurements. For this purpose, we consider the validation error Δ_{ret} using vector and scalar radiative transfer in our forward model for a set of validation sites. To detect changes of less than 0.7 % in our retrieval product for different stations, we have to correct again for individual biases per station to disentangle the error sources. For this purpose, we

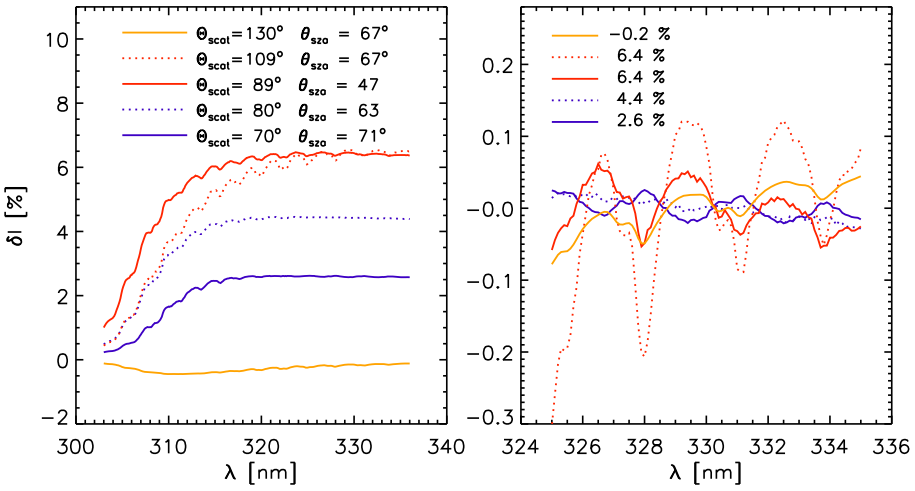

Figure 9. Relative error in the radiance simulation due to the use of scalar radiative transfer modeling for different scattering geometries. Left panel: relative radiance error $\delta I = (I_{\mathrm{scal}} - I_{\mathrm{vec}})/I_{\mathrm{vec}}$ for different scattering angles Θ_{scat} and solar zenith angles θ. Right panel: same as the left panel but zoomed in on the retrieval window. The mean error for the indicated spectral window is subtracted and reported in the figure legend. The simulations have been performed using satellite solar zenith angles and viewing angles adapted from the Lerwick validation data set for a clear sky model atmosphere and a Lambertian surface albedo of 0.1. The ozone profile has been taken from the US standard model atmosphere (NOAA, 1976).

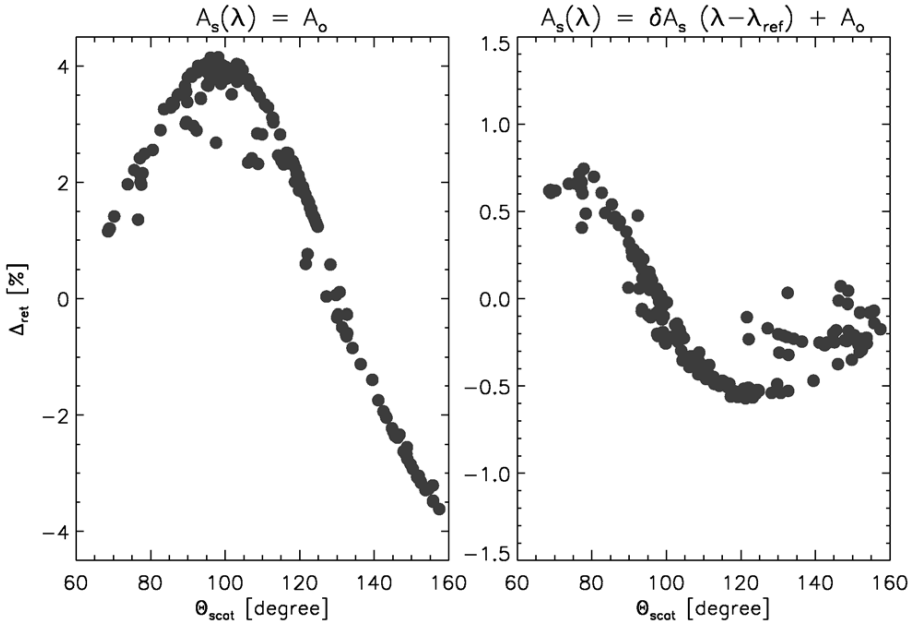

Figure 10. Ozone column error in the radiance simulation a function of single scattering angle. The retrieval error is corrected for noise contributions. Left panel: all fit parameters of our model are used next to a spectrally constant albedo. Right panel: same as the left panel but retrieving a spectrally linear dependent albedo. The simulations have been performed using the same data set as in Fig. 9.

consider validation points where the difference between using a scalar or a vector radiative transfer model $\Delta_{\mathrm{sca}} - \Delta_{\mathrm{vect}}$ is less than $\pm 0.1\,\%$ and assume that for these cases the error is dominated by a bias which does not depend on the particular radiative transfer solver. Subsequently, the mean bias of this subset is used to correct the entire validation set for the particular station. Finally, in Fig. 11, we consider the retrieval error Δ_{ret} as a function of $\Delta_{\mathrm{sca}} - \Delta_{\mathrm{vect}}$. The figure shows a clear correlation between the differences $\Delta_{\mathrm{sca}} - \Delta_{\mathrm{vect}}$ and the validation errors Δ_{ret}. For scalar radiative transfer, the differences $\Delta_{\mathrm{sca}} - \Delta_{\mathrm{vect}}$ are mapped nearly one-to-one to corresponding errors of the validation. The use of a vector radiative transfer model thus represents an improvement of the validation data set. For $\Delta_{\mathrm{sca}} - \Delta_{\mathrm{vect}} > 0.4\,\%$, the statistics

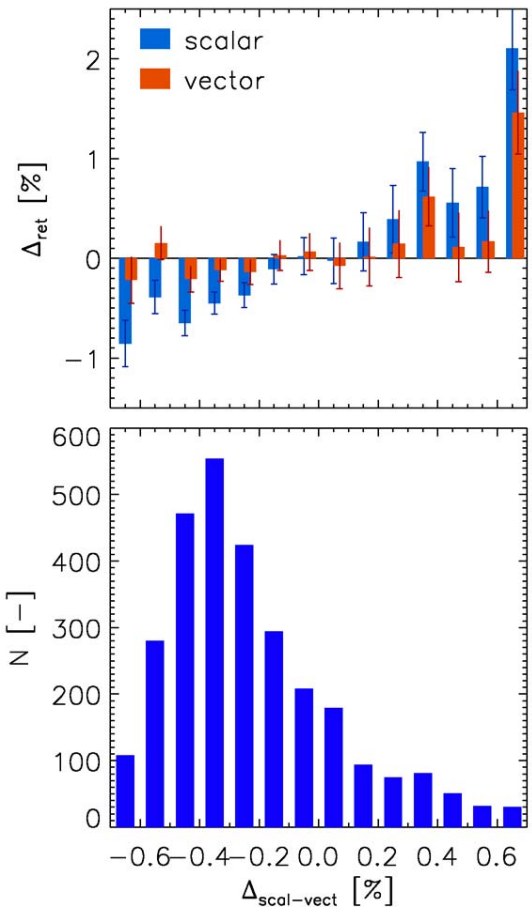

Figure 11. Effect of the radiative transfer solver on Δ_{ret}. Upper panel: total ozone column retrieval error as a function of difference between scalar and vector approach. Lower panel: number of validation points. The analysis is based on measurements at Lerwick, De Bilt, Churchill B-MKIV.032, Goose Bay, Hong Kong Obs., and Izaña.

become poor due to the fact that most validation sites are situated at latitudes higher than 50° N. Because of the sun-synchronous orbit of MetOp, this causes an asymmetric distribution of scattering angles in our data set, which might explain the larger values of Δ_{ret} for $\Delta_{sca} - \Delta_{vect} > 0.4\,\%$. Concluding on the need of vector radiative transfer to retrieve total ozone columns from the 325–335 nm UV spectral window, the induced error of less than 0.7 %, using scalar radiative transfer, has to be viewed in the context of uncertainty requirements for this data product. For example, for the future Sentinel-5 mission, an uncertainty of less then 3–5 % is required on the total ozone column product (Ingmann et al., 2012). In this context, we conclude that the use of a scalar radiative transfer solver is justified, although more accurate retrievals of the total ozone columns can be achieved using vector radiative transfer to account for the effect of polarization.

Overall, we conclude that the use of a clear sky scalar radiative transfer model using the pseudo-spherical approximation of Earth's sphericity in combination with strict cloud filtering ($\eta_{cld} < 0.1$) is fully sufficient. For this setup, Table 1 summarizes the validation using the direct comparison of ground-based and GOME-2 total ozone columns for all stations (data set 1), reporting the mean bias and the SD of the individual error as retrieval diagnostics for each station. On a global average, the difference between the observation modes of the ground-based spectrometer are small with a mean bias of −0.1 % and an error SD of 2.7 %. Overall, we see similar biases for Dobson, Brewer and SAOZ instruments with the largest biases for Scoresbysund (3.2 %), Macquarie Island (−2.3 %), and Marambio (3.3 %). In this analysis we do not account for the effective null space, and thus from the results of Fig. 13, we expect that the biases can be overestimated, as discussed in Sect. 2.2. Lerot et al. (2014) report errors due to the shape of a priori ozone profiles in the order of 1 % for solar zenith angles < 80° that can mount up to 4 % for solar zenith angles > 80°.

5 The effect of regularization

Finally, we discuss the regularization aspect of the profile scaling approach. Interpreting the retrieved column as an estimate of the true column, we showed that the direct comparison of the retrieved ozone column with ground-based measurements is subject to null space errors due to an erroneous a priori reference profile. When the retrieval product is understood as an effective column defined by Eq. (14), the null space error does not need to be considered, making the validation less dependent on the a priori choice of the reference profile. In this section, we will confirm these findings by comparing our retrieved column with ozonesondes and ground-based measurements for different choices of the reference profile.

To validate the GOME-2 effective ozone column product with collocated ozonesonde and ground-based measurements, we apply the quality criteria defined in Sect. 4.1. Here, we adopt the filter criteria of Eqs. (19)–(22) with the exception of a more stringent filtering $\delta t < 15$ DU. This reduces scattering of the validation error at the cost of the number of validation points.

Moreover, for the effective column comparison, we employ Eq. (13) and, hence, we rely on measurements of the vertical distribution of ozone, represented on the vertical grid of the model atmosphere (2 km thick model layers between 0 and 60 km). For this purpose, we use ozonesonde measurements, which are extended with the climatology of Fortuin and Kelder (1998) above the sonde burst height and subsequently normalized to the total column of ozone of a collocated ground-based measurement. This accounts for both, the lack of data above the burst height and systematic errors resulting from differences in pre-flight preparation of

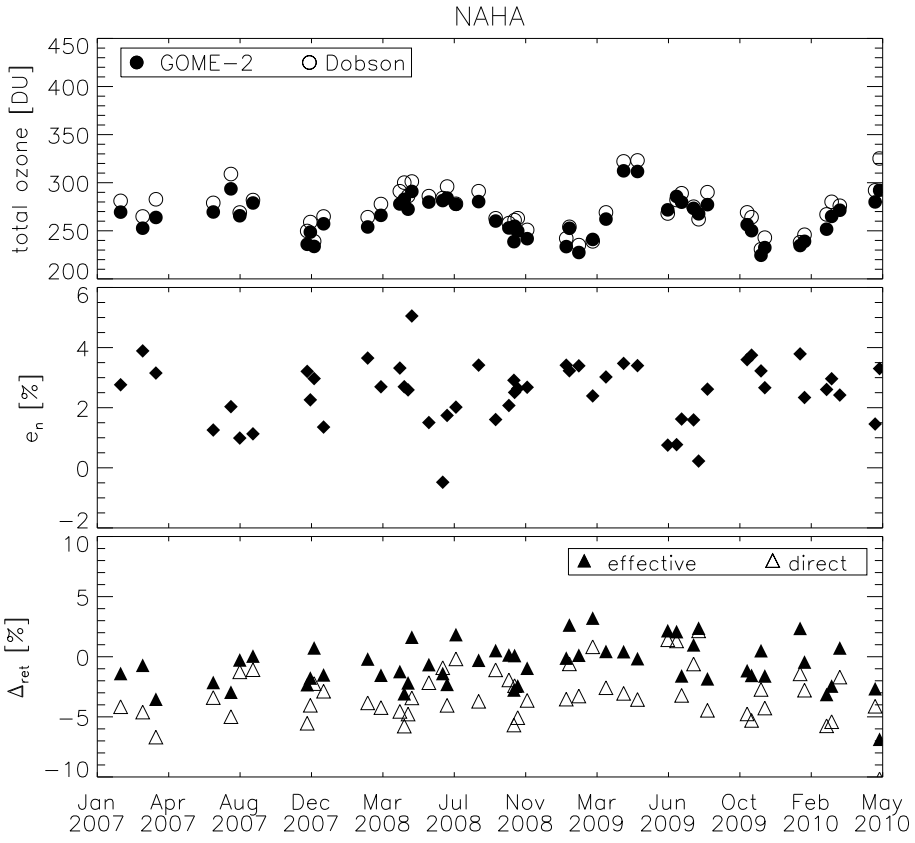

Figure 12. Time series of GOME-2 retrievals validated with ground-based Dobson direct sun measurements at Naha, Japan. Upper panel: retrieved GOME-2 total ozone column (filled circle) and the Dobson ground-based ozone column (open circle). Middle panel: the null space contribution e_n. Lower panel: the retrieval error for a direct comparison of the GOME-2 column with the Dobson column (open triangles) and for the effective column comparison accounting for the effective null space contribution e_n (Eq. 15) (filled triangles).

the ozonesonde (Kerr et al., 1994; Beekmann et al., 1994, 1995; Smit et al., 1998; Fioletov et al., 2006). Here, both ozonesonde measurements and ground-based data have to be recorded on the same day and to be spatially co-aligned to meet the quality criterion in Eq. (20). Additionally, we corrected the total column from ground-based measurements for the difference in surface elevation between the measurement site and the mean GOME-2 pixel elevation, and applied the degradation correction to GOME-2 measurements as well, as discussed before. In general, far fewer ozonesonde measurements than ground-based measurements are available, which limits the number of validation measurements. In total, 647 collocations have been found to evaluate the relevance of the total column averaging kernel.

Figure 12 displays an example of a validation of our GOME-2 total ozone column product collocated with ozonesonde measurements and Dobson direct sun measurements at Naha, Japan. The upper panel of Fig. 12 shows the time series of the retrieved total ozone column (filled circle) and the ground-based ozone column (open circle). Here, we choose the US standard reference profile to be scaled by the retrieval. Overall, we see a good agreement between both total ozone columns with the same seasonal dependence. However, a closer look reveals that the direct comparison of the ozone columns results in a negative mean bias of $-2.6\,\%$ with a SD around the mean of $2.2\,\%$. The mean bias is caused by the choice of the US standard profile as reference profile and is due to null space error, which is shown in the middle panel. The latter is estimated from the ozonesonde measurements scaled to the Dobson total ozone column and the total column averaging kernel of the individual retrievals (using Eq. 13). The null space error is $-2.6\,\%$, on average, but varies between the different soundings because of the variability of the total column averaging kernel and the ozonesonde measurements with respect to the standard atmosphere. The lower panel of Fig. 12 shows the relative retrieval error for the direct and effective column comparison. For this retrieval setting, it indicates the importance of the total column averaging kernel, where for the effective column approach the mean retrieval bias is reduced to $-0.2\,\%$ with a SD around the mean bias of $1.9\,\%$. Thus, the difference in the validation of the direct and effective column approach is due to the wrong a priori information and not due to an inadequate interpretation of the satellite measurement.

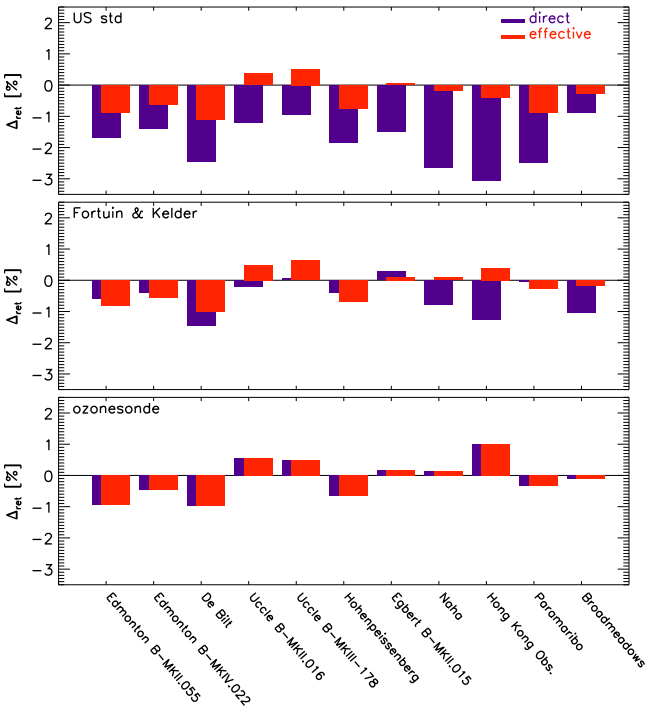

Figure 13. Mean error of the retrieved ozone column using different reference ozone profiles $\boldsymbol{\rho}_{\mathrm{ref}}$: (upper panel) adapted from the US standard atmosphere, (middle panel) from the ozone climatology of Fortuin and Kelder (1998), and (lower panel) collocated ozonesonde measurements. The red bars indicate the validation concept of the total column estimate including the total column averaging kernel and purple bars denote the direct comparison concept.

For each station from Table 1 employed in the effective column comparison, we consider the mean bias as a diagnostic tool to evaluate the effect of the choice of the reference profile. Results are depicted in Fig. 13 for a set of validation stations that comprise at least a total of 15 collocations with GOME-2 retrievals in the investigated period. We demonstrate the effect of three different choices for the reference profile in the inversion: (1) the ozone profile of the US standard atmosphere, (2) climatological profiles of Fortuin and Kelder (1998), and (3) the collocated ozonesonde measurements.

Using the US standard reference profile, the mean retrieval bias varies from station to station between −0.8 and −3 % for the direct comparison. For all sites, the bias is reduced significantly for the effective column comparison with mean biases between 0.6 and −1.1 %. For climatology profiles, the performance of both approaches becomes similar with biases ranging from 0.7 to −1 %. However, the validation of GOME-2 retrievals improves significantly for Naha, Hong Kong Observatory, and Broadmeadows for the effective column approach: from −0.8, −1.3, and 1 % (direct comparison) to 0.1, 0.4, and −0.2 % (effective column comparison), respectively. This might be caused by a deficiency in climatology by Fortuin and Kelder (1998) for these geolocations. Finally, using the ozonesonde profile as reference profile provides identical results for direct and effective column comparison with biases from 1 to −0.9 %, because the null space contribution of the reference profile vanishes (see discussion in Sect. 2.2).

Moreover, the effective column comparison results in a very similar validation for the three choices of the reference profile. For example, for Naha it varies between −0.2, 0.1, and 0.1 % for the three different reference ozone profiles. The SD of the retrieval error varies only little for the different approaches. This confirms that a proper treatment of the regularization of the profile scaling approach in the validation can reduce the dependence of the validation on the particular shape of the reference profile. For all 36 stations, we summarize the validation in Table 1 (data set 2) by giving the number of collocations, the mean error, and the error SD. Here, collocated ozonesonde measurements were used as reference profile $\boldsymbol{\rho}_{\mathrm{ref}}$.

6 Conclusions

In this paper, we presented an extensive sensitivity study for the direct fitting approach to retrieve total ozone columns from clear sky GOME-2 measurements between 325 and 335 nm. Based on an iterative least squares method, the GOME-2 reflectance measurement is fitted by adjusting the vertical ozone profile through the scaling of a reference profile, which is input to a forward model. In addition to the retrieved ozone column and its noise estimate, we provide the column averaging kernel as a retrieval product following the method of Borsdorff et al. (2014).

To account for the degradation of the GOME-2 spectrometer, we discussed a mitigation approach based on the assumption that the cloud-free mean reflectance over a certain region and a certain observation geometry and time does not change. We determined a scan-angle-dependent degradation for the period under investigation which is solely based on GOME-2 measurements that are referenced to the corresponding day in 2007 (the first year of the mission). For the eastern pixels we found a degradation of about 3–4 %, while for the western pixels the degradation is up to 9.5 % at the end of the 4.5-year period. Based on these findings we corrected the GOME-2 measurements in the period 2008–2011 and presented the improvement of our retrieval as a function of time during the first 4 years of the mission. Furthermore, we found hints to an initial calibration bias of the instrument, an aspect which has also been reported by Loyola et al. (2011).

Inherent to the direct fitting approach is the accurate simulation of GOME-2 radiances. In this context, we investigated the effect of forward model errors of the retrieval approach. We showed that the FRESCO effective cloud product (Wang et al., 2008), which is part of the disseminated level 1B data, can be used to filter GOME-2 measurements suffi-

ciently accurately for cloud contamination to justify the use of a clear sky model atmosphere for the radiative transfer simulation. Another important aspect of the forward model simulation is the representation of Earth's sphericity, and connected to that the influence of the solar zenith angle on the retrieval error. We investigated three approximations – (1) plane parallel assumption, (2) air mass correction by Kasten and Young (1989), and (3) the pseudo-spherical approximation – and found the smallest biases at large solar zenith angles ($\theta > 60^\circ$) for the pseudo-spherical approximation ranging from 2 to -1 %. Finally, we investigated the need of vector radiative transfer to simulate GOME-2 observations. Here, we showed that the use of a scalar radiative transfer model in combination with the fitting of a spectrally linear dependent Lambertian albedo can mitigate the effect of neglecting polarization and yields errors on the retrieved total ozone column < 0.7 %. With the benefit of much lower computational cost and the required uncertainties in the order of ≤ 3–5 % on the total ozone column, it is sufficient to use scalar radiative transfer together with the pseudo-spherical approximation to account for the sphericity of Earth's atmosphere.

Finally, we discussed regularization aspects of the inversion of a profile scaling approach. This allows for two different approaches interpreting the retrieved total ozone columns. First, interpreting the retrieval product as an estimate of the true column allows for a direct comparison of the retrieved column with total ozone columns from ground-based measurements but requires accurate a priori knowledge of the reference ozone profile to be scaled in the inversion. Alternatively, the retrieval product can be interpreted as an effective column defined by a vertical integration of the ozone profile using the column averaging kernel as an altitude weight. This approach accounts for the effect of the particular choice of the reference profile and, hence, both data use and validation depend less on the a priori knowledge of the relative vertical distribution of ozone. Using the pseudo-spherical approximation together with the scalar radiative transfer in our forward model to simulate clear sky measurements, we validated our retrieved column using both approaches with data from different instruments at 36 ground stations. For the direct comparison, we obtained 6861 validation measurements and found an overall bias of -0.1 % with an error SD of 2.7 %.

Furthermore, we investigated the effect of regularization of the profile scaling approach. For this purpose, we considered a set of 647 validation measurements of collocated ozonesondes, ground-based measurements and GOME-2 observations. We showed a significant dependence of the retrieval error on the choice of the reference ozone profile for the direct comparison. For example, for Naha the mean bias is -2.6, -0.8, and 0.1 % when using the ozone profile from the US standard atmosphere, the corresponding ozone profile extracted from the climatology by Fortuin and Kelder (1998), and the ozonesonde itself, respectively. This dependence is reduced significantly considering the effective ozone column: -0.2, 0.1, and 0.1 % for the different choices of the reference profile. This finding is also confirmed for other stations. It means that errors in the validation of the direct column are due to different a priori assumptions but not due to an erroneous interpretation of the GOME-2 measurements. To our knowledge, it is the first time that the role of the column averaging kernel is presented in this manner for real measurements of the total ozone column showing that the accuracy of the effective ozone column depends less on our a priori knowledge of the relative vertical ozone distribution. Furthermore, for the first time an error on the total ozone product assessed by validation is provided that is hardly affected by any error due to the choice of the a priori reference profile information. Future studies should show if the use of the column averaging kernel is useful for applications like the assimilation of the retrieved ozone column in a global or a regional model as is the case for other satellite trace gas column products (e.g., CO_2 and CH_4).

Concerning future developments of our algorithm, we envisage extending the analysis including the degradation correction for the entire mission lifetime including the application to GOME-2/METOP-B data. Moreover, we aim to increase the exploitation of the GOME-2 data set by including cloudy pixels in our data processing. For GOME measurements, van Diedenhoven et al. (2007) have shown that the combination of the UV spectral range with measurements in the O_2 A band is suited to retrieve ozone profiles for cloud contaminated measurements. We propose to investigate a similar spectral combination to retrieve the total amount of ozone simultaneously with cloud properties from GOME-2 observations.

Acknowledgements. Total ozone data as well as ozone profiles were extracted from the publicly available databases maintained by the World Ozone and Ultraviolet Radiation Data Centre (WOUDC, see www.woudc.org), the Network for the Detection of Atmospheric Composition Change (NDACC, see www.ndsc.ncep.noaa.gov), and the Southern Hemisphere ADditional OZonesondes group (SHADOZ, see http://croc.gsfc.nasa.gov/shadoz). ECMWF ERA-40 data used in this study have been acquired from the European Centre for Medium-Range Weather Forecasts data server (ECMWF, see http://apps.ecmwf.int/datasets/). We further acknowledge the reviewers for their constructive comments.

Edited by: P. Stammes

References

Antón, M., Loyola, D., López, M., Vilaplana, J. M., Bañón, M., Zimmer, W., and Serrano, A.: Comparison of GOME-2/MetOp total ozone data with Brewer spectroradiometer data over the Iberian Peninsula, Ann. Geophys., 27, 1377–1386, doi:10.5194/angeo-27-1377-2009, 2009.

Basher, R. E.: Review of the Dobson spectrophotometer and its accuracy, WMO Ozone Report 13, World Meteorological Organization, Geneva, Switzerland, 1982.

Basher, R. E.: Survey of WMO-sponsored Dobson spectrophotometer intercomparisons, WMO Ozone Report 19, World Meteorological Organization, Geneva, Switzerland, 1994.

Beekmann, M., Ancellet, G., Mégie, G., Smit, H. G. J., and Kley, D.: Intercomparison campaign of vertical ozone profiles including electrochemical sondes of ECC and Brewer–Mast type and a ground-based UV-Differential Absoption Lidar, J. Atmos. Chem., 19, 259–288, 1994.

Beekmann, M., Ancellet, G., Martin, D. C. Abonnel, C., Duverneuil, G., Eideliman, F., Bessemoulin, P., Fritz, N., and Gizard, E.: Intercomparison of tropospheric ozone profiles obtained by electrochemical sondes, a ground-based lidar, and an airborne UV-photometer, Atmos. Environ., 29, 1027–1042, 1995.

Bernhard, G., Evans, R. D., Labow, G. J., and Oltmans, S. J.: Bias in Dobson total ozone measurements at high latitudes due to approximations in calculations of ozone absorption coefficients and air mass, J. Geophys. Res., 110, D10305, doi:10.1029/2004JD005559, 2005.

Berrisford, P., Dee, D., Fielding, K., Fuentes, M., Kallberg, P., Kobayashi, S., and Uppala, S.: The ERA-Interim archive, Technical Report 1, European Centre for Medium-Range Weather Forecasts, Reading, UK, 2009

Bhartia, P. K., McPeters, R. D., Mateer, C. L., Flynn, L. E., and Wellemeyer, C.: Algorithm for the estimation of vertical ozone profile from the backscattered ultraviolet (BUV) technique, J. Geophys. Res., 101, 18793–18806, 1996.

Bhartia, P. K. and Wellemayer, C. W.: TOMS-V8 total O_3 algorithm, OMI algorithm theoretical basis document, avaliable at: http://www.knmi.nl/omi/documents/data/OMI_ATBD_Volume_2_V2.pdf (last access: 19 October 2015), 2002.

Bhartia, P. K. and Wellemayer, C. W.: TOMS v8 algorithm theoretical basis document, Technical Report, NASA, Greenbelt, Maryland, USA, 2004.

Borsdorff, T., Hasekamp, O. P., Wassmann, A., and Landgraf, J.: Insights into Tikhonov regularization: application to trace gas column retrieval and the efficient calculation of total column averaging kernels, Atmos. Meas. Tech., 7, 523–535, doi:10.5194/amt-7-523-2014, 2014.

Bovensman, H., Burrows, J. P., Buchwitz, M., Frerick, J., Noël, S., Rozanov, V. V., Chance, K. V., and Goede, A. P. H.: SCIAMACHY: mission objectives and measurement modes, J. Atmos. Sci., 56, 127–150, doi:10.1175/1520-0469(1999)056<0127:SMOAMM>2.0.CO;2, 1999.

Bramstedt, K., Noël, S., Bovensmann, H., Burrows, J. P., Lerot, C., Tilstra, L. G., Lichtenberg, G., Dehn, A., and Fehr, T.: SCIAMACHY monitoring factors: Observation and end-to-end correction of instrument performance degradation, Proceedings of the 2009 Atmospheric Science Conference, Barcelona, Spain, 7–11 September, 2009.

Brion, J., Chakir, A., Daumont, D., Malicet, J., and Parisse, C.: High-resolution laboratory absorption cross section of O_3, Temperature effect, Chem. Phys. Lett., 213, 610–612, 1993.

Bucholtz, A.: Rayleigh-Scattering calculations for the terrestrial atmosphere, Appl. Optics, 34, 2765–2773, 1995.

Burrows, J., Weber, M., Buchwitz, M., Rozanov, V., Ladstätter-Weißenmayer, A., Richter, A., DeBeek, R., Hoogen, R., Bramstedt, K., Eichmann, K.-U., Eisinger, M., and Perner, D.: The Global Ozone Monitoring Experiment (GOME): mission concept and first scientific results, J. Atmos. Sci., 56, 151–175, 1999.

Butz, A., Guerlet, S., Hasekamp, O., Schepers, D., Galli, A., Aben, I., Frankenberg, C., Hartman, J.-M., Tran, H., Kuze, A., Keppel-Aleks, G., Toon, G., Wunch, D., Wennberg, P., Deutscher, N., Griffith, D., Macatangay, R., Messerschmidt, J., Notholt, J., and Warneke, T.: Towards accurate CO_2 and CH_4 observations from GOSAT, Geophys. Res. Let., 38, L14812, doi:10.1029/2011GL047888, 2011.

Cai, Z., Liu, Y., Liu, X., Chance, K., Nowlan, C. R., Lang, R., Munro, R., and Suleiman, R.: Characterization and correction of Global Ozone Monitoring Experiment 2 ultraviolet measurements and application to ozone profile retrievals, J. Geophys. Res., 117, D07305, doi:10.1029/2011JD017096, 2012.

Coldewey-Egbers, M., Weber, M., Lamsal, L. N., de Beek, R., Buchwitz, M., and Burrows, J. P.: Total ozone retrieval from GOME UV spectral data using the weighting function DOAS approach, Atmos. Chem. Phys., 5, 1015–1025, doi:10.5194/acp-5-1015-2005, 2005.

Eskes, H. J., van der A, R. J., Brinksma, E. J., Veefkind, J. P., de Haan, J. F., and Valks, P. J. M.: Retrieval and validation of ozone columns derived from measurements of SCIAMACHY on Envisat, Atmos. Chem. Phys. Discuss., 5, 4429–4475, doi:10.5194/acpd-5-4429-2005, 2005.

Farr, T. G., Rosen, P. A., Caro, E., Crippen, R., Duren, R., Hensley, S., Kobrick, M., Paller, M., Rodriguez, E., Roth, L., Seal, D., Shaffer, S., Shimada, J., Umland, J., Werner, M., Oskin, M., Burbank, D., and Alsdorf, D.: The Shuttle Radar Topography Mission, Rev. Geophys., 45, RG2004, doi:10.1029/2005RG000183, 2007.

Fioletov, V. E., Kerr, J. B., McElroy, C. T., Wardle, D. I., Savastiouk, V., and Grajnar, T. S.: The Brewer reference triad, Geophys. Res. Lett., 32, L20805, doi:10.1029/2005GL024244, 2005.

Fioletov, V. E., Tarasick, D. W., and Petropavlovskikh, I.: Estimating ozone variability and instrument uncertainties from SBUV/2, ozonesonde, Umkehr, and SAGE II measurements: short-term variations, J. Geophys. Res., 111, D02305, doi:10.1029/2005JD006340, 2006.

Fioletov, V. E., Labow, G., Evans, R., Hare, E. W., Köhler, U., McElroy, C. T., Miyagawa, K., Redondas, A., Savastiouk, V., Shalamyansky, A. M., Staehelin, J., Vanicek, K., and Weber, M.: Performance of the ground-based total ozone network assessed using satellite data, J. Geophys. Res., 113, D14313, doi:10.1029/2008JD009809, 2008.

Fleming, E. L., Jackman, C. H., Stolarski, R. S., and Douglass, A. R.: A model study of the impact of source gas changes on the stratosphere for 1850–2100, Atmos. Chem. Phys., 11, 8515–8541, doi:10.5194/acp-11-8515-2011, 2011.

Fortuin, J. P. F. and Kelder, H.: An ozone climatology based on ozonesondes and satellite measurements, J. Geophys. Res., 103, 31709–31734, 1998.

Fuhrer, J.: Ozone risk for crops and pastures in present and future climates, Naturwissenschaften, 96, 173–194, doi:10.1007/s00114-008-0468-7, 2009.

Gloudemans, A. M. S., Schrijver, H., Hasekamp, O. P., and Aben, I.: Error analysis for CO and CH_4 total column retrievals from

SCIAMACHY 2.3 µm spectra, Atmos. Chem. Phys., 8, 3999–4017, doi:10.5194/acp-8-3999-2008, 2008.

Guicherit, R. and Roemer, M.: Tropospheric ozone trends, Chemosphere – Global Change Science, 2, 167–183, 2000.

Hao, N., Koukouli, M. E., Inness, A., Valks, P., Loyola, D. G., Zimmer, W., Balis, D. S., Zyrichidou, I., Van Roozendael, M., Lerot, C., and Spurr, R. J. D.: GOME-2 total ozone columns from MetOp-A/MetOp-B and assimilation in the MACC system, Atmos. Meas. Tech., 7, 2937–2951, doi:10.5194/amt-7-2937-2014, 2014.

Hasekamp, O. and Landgraf, J.: Ozone profile retrieval from backscattered ultraviolet radiances: the inverse problem solved by regularization, J. Geophys. Res., 106, 8077–8088, doi:10.1029/2000JD900692, 2001.

Hasekamp, O. P. and Landgraf, J.: Linearization of vector radiative transfer with respect to aerosol properties and its use in satellite remote sensing, J. Geophys. Res., 110, D04203, doi:10.1029/2004JD005260, 2005.

Hoogen, R., Rozanov, V., and Burrows, J.: Ozone profiles from GOME satellite data: algorithm description and first validation, J. Geophys. Res., 104, 8263–8280, 1999.

Ingmann, P., Veihelmann, B., Langen, J., Lamarre, D., Stark, H., and Courrèges-Lacoste, G. B.: Requirements for the GMES Atmosphere Service and ESA's implementation concept: Sentinels-4/-5 and -5p, Remote Sens. Environ., 120, 58–59, doi:10.1016/j.rse.2012.01.023, 2012.

Joiner, J., Bhartia, P. K., Cebula, R. P., Hilsenrath, E., McPeters, R. D., and Park, H.: Rotational Raman scattering (Ring effect) in satellite backscatter ultraviolet measurements, Appl. Optics, 34, 4513–4525, 1995.

Kasten, F. and Young, T.: Revised optical air mass tables and approximation formula, Appl. Optics, 28, 4375, doi:10.1364/AO.28.004735, 1989.

Kerr, J. B., Fast, H., McElroy, C. T., Oltmans, S. J., Lathrop, J. A., Kyrö, E., Paukkunen, A., Claude, H., Köhler, U., Sreedharan, C. R., Takao, T., and Tsukagoshi, Y.: The 1991 WMO international ozonesonde intercomparison at Vanscoy, Canada, Atmos. Ocean, 32, 685–716, doi:10.1080/07055900.1994.9649518, 1994.

Kerr, J. B., McElroy, C. T., and Wardle, D. W.: The Brewer instrument calibration center 1984–1996, in: Atmospheric Ozone: Proceedings of the XVIII Ozone Symposium, Parco Sci., and Tecnologico D' Abruzzo, L'Aquila, Italy, 915–918, 1997.

Komhyr, W. D., Grass, R. D., and Leonard, R. K.: Dobson spectrophotometer 83: a standard for total ozone measurements 1963–1987, J. Geophys. Res., 94, 9847–9861, 1989.

Koukouli, M. E., Balis, D. S., Loyola, D., Valks, P., Zimmer, W., Hao, N., Lambert, J.-C., Van Roozendael, M., Lerot, C., and Spurr, R. J. D.: Geophysical validation and long-term consistency between GOME-2/MetOp-A total ozone column and measurements from the sensors GOME/ERS-2, SCIAMACHY/ENVISAT and OMI/Aura, Atmos. Meas. Tech., 5, 2169–2181, doi:10.5194/amt-5-2169-2012, 2012.

Krijger, J. M., Aben, I., and Landgraf, J.: CHEOPS-GOME: WP2.1: study of instrument degradation, Report SRON-EOS/RP/05-018, European Space Agency, Paris, France, 2005.

Lacis, A. A., Chowdhary, J., Mishchenko, M. I., and Cairns, B.: Modeling errors in diffuse-sky radiation: Vector vs scalar treatment, Geophys. Res. Lett., 25, 135–138, 1998.

Landgraf, J., Hasekamp, O. P., Box, M. A., and Trautmann, T.: A linearized radiative transfer model for ozone profile retrieval using the analytical forward-adjoint pertubation theory approach, J. Geophys. Res., 106, 27291–27305, 2001.

Landgraf, J., Hasekamp, O. P., van Deelen, R., and Aben, I.: Rotational Raman scattering of polarized light in the Earth atmosphere: a vector radiative transfer model using the radiative transfer perturbation theory approach, J. Quant. Spectrosc. Ra., 87, 399–433, doi:10.1016/j.jqsrt.2004.03.013, 2004.

Lerot, C., van Roozendael, M., Lambert, J.-C., Granville, J., van Gent, J., Loyola, D., and Spurr, R.: The GODFIT algorithm: a direct fitting approach to improve the accuracy of total ozone measurementsfrom GOME, Int. J. Remote Sens., 31, 543–550, doi:10.1080/01431160902893576, 2010.

Lerot, C., van Roozendael, M., Spurr, R., Loyola, D., Coldewey-Egbers, M., Kochenova, S., van Gent, J., Koukouli, M., Balis, D., Lambert, J.-C., Granville, J., and Zehner, C.: Homogenized total ozone data records from the European sensors GOME/ERS-2, SCIAMACHY/Envisat, and GOME-2/MetOp-A, J. Geophys. Res., 119, 1639–1662, doi:10.1002/2013JD020831, 2014.

Levelt, P. F., van den Oord, G. H. J., Dobber, M. R., Mälkki, A., Visser, H., de Vries, J., Stammes, P., Lundell, J. O. V., and Saari, H.: The ozone monitoring instrument, IEEE T. Geosci. Remote, 44, 1093–1101, doi:10.1109/TGRS.2006.872333, 2006.

Liu, X., Chance, K., and Kurosu, T. P.: Improved ozone profile retrievals from GOME data with degradation correction in reflectance, Atmos. Chem. Phys., 7, 1575–1583, doi:10.5194/acp-7-1575-2007, 2007.

Loyola, D. G., Koukouli, M. E., Valks, P., Balis, D. S., Hao, N., Van Roozendael, M., Spurr, R. J. D., Zimmer, W., Kiemle, S., Lerot, C., and Lambert, J.-C.: The GOME-2 total column ozone product: retrieval algorithm and ground-based validation, J. Geophys. Res., 116, D07302, doi:10.1029/2010JD014675, 2011.

McPeters, R. D., Labow, G. J., and Logan, J. A.: Ozone climatological profiles for satellite retrieval algorithms, J. Geophys. Res., 112, D05308, doi:10.1029/2005JD006823, 2007.

Mishchenko, M. I., Lacis, A. A., and Travis, L. D.: Errors induced by the neglect of polarization in radiance calculations for Rayleigh-scattering atmospheres, J. Quant. Spectrosc. Ra., 51, 491–510, 1994.

Munro, R., Lang, R., Klaes, D., Poli, G., Retscher, C., Lindstrot, R., Huckle, R., Lacan, A., Grzegorski, M., Holdak, A., Kokhanovsky, A., Livschitz, J., and Eisinger, M.: The GOME-2 instrument on the Metop series of satellites: instrument design, calibration, and level 1 data processing – an overview, Atmos. Meas. Tech. Discuss., 8, 8645–8700, doi:10.5194/amtd-8-8645-2015, 2015.

NOAA: US Standard Atmosphere, 1976, Technical Report NOAA-S/T76-1562, National Oceanic and Atmospheric Administration, US Gov. Printing Office, Washington, DC, USA, 1976.

Noël, S., Bramstedt, K., Bovensmann, H., Burrows, J. P., Gottwald, M., and Krieg, E.: SCIAMACHY degradation monitoring results, Proceedings of the 2007 Envisat Symposium, Montreux, Switzerland, 23–27 April, 2007.

Pawson, S., Steinbrecht, W., Charlton-Perez, A. J., Fujiwara, M., Karpechko, A. Yu., Petropavlovskikh, I., Urban, J., and Weber, M.: Update on global ozone: Past, present, and future, Chapter 2 in Scientific Assessement of Ozone Depletion: 2014, Global

Ozone Research and Monitoring Project – Report No. 55, World Meteorological Organization, Geneva, Switzerland, 2014.

Pfeilsticker, K., Erle, F., Funk, O., Marquard, L., Wagner, T., and Platt, U: Optical path modifications due to tropospheric clouds: Implications for zenith sky measurements of stratospheric gases, J. Geophys. Res.-Atmos., 103, 25323–25335, 1998.

Rodgers, C. D.: Inverse Methods for Atmospheres: Theory and Practice, vol. 2, World Scientific, Singapore, New Jersey, London, Hong Kong, 2000.

Schepers, D., aan de Brugh, J. M. J., Hahne, Ph., Butz, A., Hasekamp, O. P., and Landgraf, J.: LINTRAN v2.0: a linearised vector radiative transfer model for efficient simulation of satellite-born nadir-viewing reflection measurements of cloudy atmospheres, J. Quant. Spectrosc. Ra., 149, 347–359, doi:10.1016/j.jqsrt.2014.08.019, 2014.

Smit, H. G. J. and Kley, D.: JOSIE: The 1996 WMO international intercomparison of ozonesondes under quasi flight conditions in the environmental simulation chamber at Jülich, WMO Global Atmosphere Watch report series, No. 130 (Technical Document No. 926), World Meteorological Organization, Geneva, Switzerland, 1998.

Snel, R.: In-orbit optical path degradation: GOME experience and SCIAMACHY prediction, ERS Envisat Symposium, SP-461, Göteborg, Sweden, 2000.

Staehelin, J., Kerr, J., Evans, R., and Vanicek, K.: Comparison of total ozone measurements of Dobson and Brewer spectrophotometers and recommended transfer functions, Report WMO TD 1147, World Meteorological Organization, Geneval, Switzerland, 2003.

Stammes, P.: Errors in UV reflectivity and albedo calculations due to neglecting polarization, in: Proceedings of the European Symposium on Satellite Remote Sensing, vol. 2311, p. 21, EOS/SPIE, Rome, Italy, 1994.

Tanzi, C. P., Snel, R., Hasekamp, O., and Aben, I.: Degradation of UV earth albedo observations by GOME, ERS Envisat Symposium, SP-461, Göteborg, Sweden, 2000.

Thompson, A. M., Witte, J. C., Smit, H. G. J., Oltmans, S. J., Johnson, B. J., Kirchhoff, V. W. J. H., and Schmidlin, F. J.: Southern Hemisphere Additional Ozonesondes (SHADOZ) 1998–2004 tropical ozone climatology: 3. Instrumentation, station-to-station variability, and evaluation with simulated flight profiles, J. Geophys. Res., 112, D03304, doi:10.1029/2005JD007042, 2007.

Tilstra, L. G., de Graaf, M., Aben, I., and Stammes, P.: In-flight degradation correction of SCIAMACHY UV reflectances and Absorbing Aerosol Index, J. Geophys. Res., 117, D06209, doi:10.1029/2011JD016957, 2012.

Tilstra, L. G., Tuinder, O. N. E., and Stammes, P.: A new method for in-flight degradation correction of GOME-2 Earth reflectance measurements, with application to the absorbing aerosol index, Proceedings of the EUMETSAT Satellite Conference, Sopot, Poland, 2–7 September, 2012.

van Deelen, R., Landgraf, J., and Aben, I.: Multiple elastic and inelastic light scattering in the Earth's atmosphere: a doubling-adding method to include rotational Raman scattering by air, J. Quant. Spectrosc. Ra., 95, 309–330, doi:10.1016/j.jqsrt.2004.11.002, 2005.

van Deelen, R., Hasekamp, O. P., and Landgraf, J.: Accurate modeling of spectral fine-structure in Earth radiance spectra measured with the Global Ozone Monitoring Experiment, Appl. Optics, 46, 243–252, doi:10.1364/AO.46.000243, 2007.

van der A, R. J., van Oss, R. F., Piters, A. J. M., Fortuin, J. P. F., Meijer, Y. F., and Kelder, H. M.: Ozone profile retrieval from recalibrated Global Ozone Monitoring Experiment data, J. Geophys. Res., 107, 4239, doi:10.1029/2001JD000696, 2002.

van Diedenhoven, B., Hasekamp, O. P., and Landgraf, J.: Retrieval of cloud parameters from satellite-based reflectance measurements in the ultraviolet and the oxygen A-band, J. Geophys. Res., 112, D15208, doi:10.1029/2006JD008155, 2007.

van Roozendael, M., Peeters, P., Roscoe, H. K., De Backer, H., Jones, A. E., Bartlett, L., Vaughan, G., Goutail, F., Pommereau, J.-P., Kyrö, E., Wahlstrom, C., Braathen, G., and Simon, P. C.: Validation of ground-based visible measurements of total ozone by comparison with Dobson and Brewer spectrophotometers, J. Atmos. Chem., 29, 55–83, 1998.

van Roozendael, M., Loyola, D., Spurr, R., Balis, D., Lambert, J.-C., Livschitz, Y., Valks, P., Ruppert. T., Kenter, P., Fayt, C., and Zehner, C.: Ten years of GOME/ERS-2 total ozone data – the new GOME data processor (GDP) version 4: 1. Algorithm description, J. Geophys. Res., 111, D14311, doi:10.1029/2005JD006375, 2006.

van Roozendael, M., Spurr, R., Loyola, D., Lerot, C., Balis, D., Lambert, J.-C., Zimmer, W., van Gent, J., van Geffen, J., Koukouli, M., Granville, J., Doicu, A., Fayt, C., and Zehner, C.: Sixteen years of GOME/ERS-2 total ozone data: The new direct fitting GOME data processor (GDP) version 5 – Algorithm description, J. Geophys. Res., 117, D03305, doi:10.1029/2011JD016471, 2012.

van Soest, G., Tilstra, L. G., and Stammes, P.: Large-scale validation of SCIAMACHY reflectance in the ultraviolet, Atmos. Chem. Phys., 5, 2171–2180, doi:10.5194/acp-5-2171-2005, 2005.

Veefkind, J. P., De Haan, J., Brinksma, E., Kroon, M., and Levelt, P.: Total ozone from the Ozone Monitoring Instrument (OMI) using the OMI-DOAS technique, IEEE T. Geosci. Remote, 44, 1239–1244, doi:10.1109/TGRS.2006.871204, 2004.

Vidot, J., Landgraf, J., Hasekamp, O. P., Butz, A., Galli, A., Tol, P., and Aben, I.: Carbon monoxide from shortwave infrared reflectance measurements: A new retrieval approach for clear sky and partially cloudy atmospheres, Remote Sens. Environ., 120, 255–266, doi:10.1016/j.rse.2011.09.032, 2012.

Walter, H. H., Landgraf, J., and Hasekamp, O. P.: Linearization of a pseudo-spherical vector radiative transfer model, J. Quant. Spectrosc. Ra., 85, 251–283, doi:10.1016/S0022-4073(03)00228-0, 2004.

Wang, P., Stammes, P., van der A, R., Pinardi, G., and van Roozendael, M.: FRESCO+: an improved O_2 A-band cloud retrieval algorithm for tropospheric trace gas retrievals, Atmos. Chem. Phys., 8, 6565–6576, doi:10.5194/acp-8-6565-2008, 2008.

Weber, M., Lamsal, L. N., Coldewey-Egbers, M., Bramstedt, K., and Burrows, J. P.: Pole-to-pole validation of GOME WFDOAS total ozone with groundbased data, Atmos. Chem. Phys., 5, 1341–1355, doi:10.5194/acp-5-1341-2005, 2005.

World Health Organization (WHO): Health aspects of air pollution with particulate matter, ozone and nitrogen dioxide: report on a WHO working group, 13–15 January 2003, Bonn, Germany, WHO Regional Office for Europe, Copenhagen, Denmark, EUR/03/5042688, 2003.

World Meteorological Organization (WMO): Scientific assessment of ozone depletion, World Meteorological Organization, Genova, Switzerland, Global Ozone Research and Monitoring Project-Report No. 55, 416 pp. 2014.

Ziemke, J. R., Chandra, S., Labow, G. J., Bhartia, P. K., Froidevaux, L., and Witte, J. C.: A global climatology of tropospheric and stratospheric ozone derived from Aura OMI and MLS measurements, Atmos. Chem. Phys., 11., 9237–9251, doi:10.5194/acp-11-9237-2011, 2011.